DU[illegible]
NAV[illegible]
MONTEREY, CALIFORNIA 93943

NAVAL POSTGRADUATE SCHOOL
Monterey, California

THESIS

CHARACTERIZATIONS OF PREHEATED AND
NON-PREHEATED HY-80 STEEL WELDMENTS
BY TRANSMISSION ELECTRON MICROSCOPY

by

David Richard Clark

September 1983

Thesis Advisor: K. D. Challenger

Approved for public release; distribution unlimited.

T215129

REPORT DOCUMENTATION PAGE

READ INSTRUCTIONS BEFORE COMPLETING FORM

1. REPORT NUMBER

2. GOVT ACCESSION NO.

3. RECIPIENT'S CATALOG NUMBER

4. TITLE (and Subtitle)
Characterizations of Preheated and Non-Preheated HY-80 Steel Weldments by Transmission Electron Microscopy

5. TYPE OF REPORT & PERIOD COVERED
Master's Thesis; September 1983

6. PERFORMING ORG. REPORT NUMBER

7. AUTHOR(s)
David Richard Clark

8. CONTRACT OR GRANT NUMBER(s)

9. PERFORMING ORGANIZATION NAME AND ADDRESS
Naval Postgraduate School
Monterey, California 93943

10. PROGRAM ELEMENT, PROJECT, TASK AREA & WORK UNIT NUMBERS

11. CONTROLLING OFFICE NAME AND ADDRESS
Naval Postgraduate School
Monterey, California 93943

12. REPORT DATE
September 1983

13. NUMBER OF PAGES
95

14. MONITORING AGENCY NAME & ADDRESS(if different from Controlling Office)

15. SECURITY CLASS. (of this report)
Unclassified

15a. DECLASSIFICATION/DOWNGRADING SCHEDULE

16. DISTRIBUTION STATEMENT (of this Report)
Approved for public release; distribution unlimited.

17. DISTRIBUTION STATEMENT (of the abstract entered in Block 20, if different from Report)

18. SUPPLEMENTARY NOTES

19. KEY WORDS (Continue on reverse side if necessary and identify by block number)
HY-80 Steel Weldments

20. ABSTRACT (Continue on reverse side if necessary and identify by block number)
Preheating HY-80 steel weldments is standard procedure, but it is an expensive and time consuming step in the fabrication of hull structures. The microstructures and hardness profiles of both a preheated (250° F--121° C) and a non-preheated (32° F--0° C) HY-80 steel weldment were studied to provide information and allow comparisons of the microstructural transformations that occur in the heat affected zone during shielded metal arc welding.

#20 - ABSTRACT - (CONTINUED)

Optical, scanning electron and transmission electron microscopy were utilized to characterize the microstructure within the heat affected zone of each weldment. The only significant difference observed was that preheating reduced the amount of transformation twinned martensite found in the weld heat affected zone which may reduce the susceptibility to hydrogen induced cold cracking.

Approved for public release; distribution unlimited.

Characterizations of Preheated and Non-Preheated HY-80 Steel Weldments by Transmission Electron Microscopy

by

David Richard Clark
Lieutenant Commander, United States Navy
B.S., Purdue University, 1975
M.P.A., University of Mississippi, 1981

Submitted in partial fulfillment of the requirements for the degree of

MASTER OF SCIENCE IN MECHANICAL ENGINEERING

from the

NAVAL POSTGRADUATE SCHOOL

September 1983

DUDLEY KNOX LIBRARY
NAVAL POSTGRADUATE SCHOOL
MONTEREY, CALIFORNIA 93943

ABSTRACT

Preheating HY-80 steel weldments is standard procedure, but it is an expensive and time consuming step in the fabrication of hull structures. The microstructures and hardness profiles of both a preheated (250° F--121° C) and a non-preheated (32° F--0° C) HY-80 steel weldment were studied to provide information and allow comparisons of the microstructural transformations that occur in the heat affected zone during shielded metal arc welding. Optical, scanning electron and transmission electron microscopy were utilized to characterize the microstructure within the heat affected zone of each weldment. The only significant difference observed was that preheating reduced the amount of transformation twinned martensite found in the weld heat affected zone which may reduce the susceptibility to hydrogen induced cold cracking.

TABLE OF CONTENTS

I. INTRODUCTION ---------- 10

II. BACKGROUND ---------- 13

III. EXPERIMENTAL PROCEDURE ---------- 24

IV. EXPERIMENTAL RESULTS ---------- 37

V. DISCUSSION ---------- 81

VI. CONCLUSIONS ---------- 89

VII. RECOMMENDATIONS ---------- 91

LIST OF REFERENCES ---------- 92

INITIAL DISTRIBUTION LIST ---------- 95

LIST OF TABLES

1. Chemical Composition Limits of HY-80 Steel Plate ---------- 14

2. Mechanical Property Limits of HY-80 Steel Plate ---------- 16

3. Minimum Preheat Temperatures for Welding HY-80 Steel Plate ---------- 19

4. Chemical Composition Limits of 11018 Alloy Rod Electrode ---------- 25

5. Mechanical Property Limits of 11018 Alloy Rod Electrode ---------- 26

6. Wafer Locations in Preheated HY-80 Steel Weldment ---------- 32

7. Wafer Locations in Non-Preheated HY-80 Steel Weldment ---------- 32

LIST OF FIGURES

1. Time-Temperature-Transformation Curves for HY-80 Steel ---------- 17
2. Macrosample of Preheated HY-80 Steel Weldment ----- 28
3. Macrosample of Non-Preheated HY-80 Steel Weldment - 28
4. Wafer Cutting Locations from Preheated Weldment --- 29
5. Wafer Cutting Locations from Non-Preheated Weldment ---------- 30
6. Three Dimensional Topography of HY-80 Steel Weldment ---------- 33
7. Microstructure Mapping for TEM Thin Foil Sample Selection ---------- 36
8. Vickers Hardness Traverse of Preheated Weldment --- 38
9. Vickers Hardness Traverse of Non-Preheated Weldment ---------- 41
10. Optical Micrograph of Location A ---------- 44
11. SEM Micrograph of Location A ---------- 44
12. TEM Micrographs of Location A ---------- 45
13. Optical Micrograph of Location B ---------- 49
14. SEM Micrograph of Location B ---------- 49
15. TEM Micrographs of Location B ---------- 50
16. Optical Micrograph of Location C ---------- 53
17. SEM Micrograph of Location C ---------- 53
18. TEM Micrographs of Location C ---------- 55
19. Optical Micrograph of Location D ---------- 58
20. SEM Micrograph of Location D ---------- 58
21. TEM Micrographs of Location D ---------- 59

22. Optical Micrograph of Location E ---------- 63

23. SEM Micrograph of Location E ---------- 63

24. TEM Micrographs of Location E ---------- 64

25. Optical Micrograph of Locations B' and C' --------- 68

26. SEM Micrograph of Location B' ---------- 68

27. TEM Micrographs of Location B' ---------- 69

28. SEM Micrograph of Location C' ---------- 72

29. TEM Micrographs of Location C' ---------- 73

30. Optical Micrograph of Location D' and E' ---------- 77

31. SEM Micrograph of Location D' ---------- 77

32. TEM Micrographs of Location D' ---------- 78

33. Average Diameter of Preheated Temper Carbides ----- 82

34. Average Diameter of Non-Preheated Temper Carbides - 83

35. Average Martensite Lath Width of the Preheated Weldment ---------- 87

36. Average Martensite Lath Width of the Non-Preheated Weldment ---------- 88

ACKNOWLEDGMENTS

I wish to express my sincere appreciation to my thesis advisor, Professor K.D. Challenger, for his guidance in this research effort. I would also like to thank Dr. Prabir Deb and Mr. Tom Kellogg for their assistance in the laboratory.

Special thanks is extended to my wife, Christine and my daughters Carey and Lisa for their patience and understanding throughout the course of my graduate studies.

I. INTRODUCTION

HY-80 is the U.S. Navy designation for a quenched and tempered, low carbon, nickel, chromium, molybdenum steel with a minimum yield strength of 80 Ksi (550 MPa). It has an excellent strength to weight ratio, excellent notch toughness at low temperatures, and good antiballistic properties making it the primary material in the construction of nuclear submarine pressure hulls. The strength and toughness is achieved by the heat treatment process employed during manufacture which creates a fully tempered low carbon martensitic/bainitic structure. HY-80 is manufactured to the following military specifications:

1. Plate: MIL-S-16216
2. Extrusions: MIL-S-22664
3. Rolled Sections: MIL-S-22958
4. Castings: MIL-S-23008
5. Forgings: MIL-S-23009

Fusion welding is the principle joining technique employed in the construction of submarine pressure hulls. Understanding the effects of the welding process on the structure and mechanical properties of an HY-80 Weldment is of extreme importance.

A marked impairment in the fracture toughness of HY-80 is observed in the base metal area adjacent to the molten

weld area. This weld heat affected zone (HAZ) undergoes microstructural transformations due to the thermal cycling that occurs during the welding process; these changes in microstructure contribute to an increased susceptibility to both brittle fracture and hydrogen induced cold cracking. By control and proper selection of the many welding variables such as welding process, heat input, electrodes, fluxes, preheat, etc., acceptable levels of toughness and strength can be achieved in the finished weld. It is the purpose of this study to characterize and compare the microstructures of the heat affected zones of both a preheated (250° F--121° C) HY-80 Steel SMA weldment and a non preheated (32° F--0° C) HY-80 steel SMA weldment. At present the welding procedure for HY-80 requires a 250° F (120° C) preheat for several reasons which include a reduction in the cooling rate following welding which allows more autotempering of the martensite that forms, allows some of the hydrogen introduced during welding to diffuse out of the weldment and reduces the possibility of hydrogen dissolution by removing some of the sources for hydrogen such as moisture on the metal prior to welding. Preheating is an expensive and time consuming step in the fabrication of hull structures; this has motivated the development of improved welding rods that will reduce the amount of hydrogen introduced during welding.

The characterization of the weldments performed in this thesis has been done in order to determine if there are any

undesirable microstructural changes that occur when pre-heating is eliminated.

II. BACKGROUND

HY-80 was the first high-strength quenched and tempered steel approved for use by the U.S. Navy for construction of large ocean vessels. The high strength, good fracture toughness and good weldability of HY-80 are its primary advantages over its predecessor, low carbon HTS steel. Additionally, HY-80 requires no post weld heat treatment when established welding procedures are followed. Welding procedures for HY-80 are governed by military specifications MIL-S-19322, [Ref. 1]. Production of HY-80 plate steel is governed by MIL-S-16216, [Ref. 2]. The chemical composition limits of HY-80 are shown in Table 1.

The alloying elements each serve an important role in establishing the mechanical properties of HY-80. Carbon is maintained below 0.18% to ensure good weldability while achieving the desired strength levels. Nickel is added primarily to increase the hardenability.

It is observed that nickel also lowers the nil ductility temperature (NDT) of HY-80 steel [Ref. 3]. The range of 2 to 3.25% nickel is a compromise to achieve hardenability while maintaining its weldability. Chromium is also added to increase the hardenability and secondary hardening during the tempering treatment of HY-80 steel. The limits are set between 1.0--1.80% to act as a carbide former in hardening

TABLE I

CHEMICAL COMPOSITION LIMITS OF HY-80 STEEL PLATE (PERCENT)

ELEMENT	MIL-S-16216 HY-80	COMMERCIAL A543 GRADE A
Carbon[a]	0.18 max.	0.23 max.
Manganese	0.10--0.40	0.40 max.
Silicon	0.15--0.35	0.20--0.35
Nickel	2.00--3.25	2.60--3.25
Chromium	1.00--1.80	1.50--2.00
Molybdenum	0.20--0.60	0.45--0.60
Phosphorous[b]	0.025 max.	0.035 max.
Sulfur[b]	0.025 max.	0.040 max.
Titanium	0.02 max.	--
Vanadium	0.03 max.	0.03 max.
Copper	0.25 max.	--
Iron	Remainder	Remainder

[a] 0.20 maximum for plates 6 inches thick and over.

[b] The percent of combined phosphorous and sulfur shall be 0.045 max.

the steel. Chromium also improves the corrosion resistance of HY-80 steel. Phosphorous and sulfur are both detrimental elements. Sulfur combines with iron to form iron-sulfide, which liquifies at normal rolling and forging temperatures. Manganese addition prevents the formation of iron-sulfide by preferentially forming manganese-sulfide, thereby limiting the sulfur available for reaction with iron. The manganese also solid solution strengthens the steel. Excess manganese causes embrittlement so its content is restricted to a maximum of 0.40%. Molybdenum is used to increase the temper resistance, improving hardenability, creep resistance, and machineability. Silicon is added to act as a deoxidizer.

HY-80 is a fully killed, low alloy steel which acquires its strength and toughness through quenching and tempering. The resulting microstructure of the as-received HY-80 is a combination of tempered bainite and tempered martensite throughout the plate. MIL-S-16216 lists only two limitations regarding the procedures for the quenching and tempering heat treatments required in the production of HY-80 steel. The first is to establish the final tempering temperature as not less than 1100° F, and the second is that the mid-thickness microstructure shall contain not less than 80% martensite. The mechanical property specification limits of HY-80 steel are shown in Table 2. The time-temperature-transformation diagram shown in Figure 1, illustrates the sluggishness of the austenite decomposition.

TABLE 2

MECHANICAL PROPERTY LIMITS OF HY-80 STEEL PLATE

PROPERTY	MIL-S-16216 HY-80	COMMERCIAL A543 GRADE A
Tensile Strength (ksi)	NS[a]	105/125
Yield Strength 0.2% offset (ksi)	80/95[b]	85 min.
Elongation in 2 in. min. percent	20[b]	14
Reduction in Area min. percent		
Longitudinal	55[b]	NS
Transverse	50[b]	NS
Charpy V-notch min. impact (ft-lbs)		
1/2 to 2 in.	50 @ -120° F	NS
over 2 in.	30 @ -120° F	NS

[a] NS--not specified.

[b] These values for plate thicknesses 5/8 inch and over.

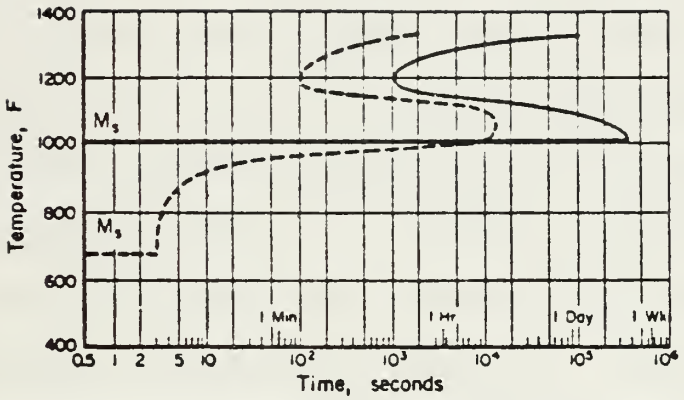

	Solid Curve	Dotted Curve
C	0.16	0.13
Mn	0.34	0.16
P	0.014	0.009
S	0.024	0.013
Si	0.25	0.10
Ni	2.87	3.08
Cr	1.52	1.76
Mo	0.41	0.49
Austenitizing Temperature	2400 F	1650 F

Source: Published information in Reference 4.

Figure 1. Time-Temperature-Transformation Curves for HY-80

Emmanuel, Young, and Spahr [Ref. 4] developed this diagram to illustrate these transformations as a function of austenitizing temperature. The slow response to transformation results in a duplex microstructure consisting of martensite and bainite, typically found in HY-80 steel plate.

A significant portion of the cost of ship construction is attributed to welding. It has been estimated as high as 50% of the total manhours spent in hull fabrication is associated with welding [Ref. 5]. HY-80 is considered very weldable and it displays good as-welded characteristics when welded following established procedures. However, any refinements improving the fabrication methods of HY-80 will be realized many times over due to the labor intensive nature of welding. Several studies have been conducted to determine the effects of the heat input during welding. These investigations are well documented in the literature [Refs. 6-12]. Smith [Ref. 13] concluded that the fracture toughness in the grain coarsened heat affected zone was impaired due to the welding process. However it was also reported that this impairment was least severe when welding at higher heat inputs. This results from the formation of a slightly lower hardness martensite. Preheating HY-80 steel prior to welding is a standard welding practice. The minimum amount of preheat necessary is dependent on the plate thickness to be welded, as shown in Table 3. Preheating is necessary for the prevention of hydrogen entrapment in the

TABLE 3

MINIMUM PREHEAT TEMPERATURES FOR WELDING HY-80 STEEL PLATE

PLATE THICKNESS (in.)	MINIMUM PREHEAT OR INTERPASS TEMPERATURE (°F)
up to 1/2	75
1/2 to 1 1/8	125
over 1 1/8	200

weldment and to aid in preventing weld-metal cracking in restrained welds.

Electrode development paralleled the development of HY-80 steel. Government specifications MIL-E-22200 provide proper electrode designations for welding HY-80. Electrodes used in shielded metal-arc welding (SMAW) of HY-80 steel are of the low hydrogen type. Materials containing little or no hygroscopic elements are used in the flux covering of these type electrodes. The protective atmosphere is generated by burning inorganic materials in the flux covering such as calcium carbonate [Ref. 14]. Electrode handling and storage is critical to ensure no moisture (a source of hydrogen) is introduced into the welding process. The electrode filler metal is selected such that the as-cast weld metal will possess similar characteristics as the fully heat treated base metal. When the established welding procedures are followed the joining of HY-80 steel by welding is quite

satisfactory. Whenever these techniques or proper materials are not employed hydrogen induced cold cracking becomes a prominent problem. The problem of hydrogen induced cracking in the apparent HAZ is still unresolved. Many studies have been conducted to piece together the causes and mechanisms of hydrogen induced cold cracking [Refs. 15,16,17,18,19]. Certain microstructures appear to be linked to the susceptibility to hydrogen induced cracking. Savage, Nippes, and Szekeres [Ref. 20], investigated the size, shape, and distribution of sulfide inclusions and their relationship to cold cracking. They generalized the cold cracking problem as containing four factors as follows: (1) cracks usually appear to be associated with the weld/fusion boundary, (2) variations in crack susceptibility can exist among heats with the same nominal compositions, (3) hydrogen plays a very significant role in the cracking, and (4) stresses of the order of the yield strength must be present. Porter and Easterling [Ref. 21] reported findings that welding high strength steels in the presence of hydrogen caused consistent failures in the HAZ. Hydrogen can be absorbed into the molten weld metal from where it quickly diffuses into the HAZ. During the subsequent cooling of the weldment, which in effect is quenched by the mass of the much cooler base metal acting as a heat sink, martensite is readily formed. Beachem [Ref. 22] presents a model for hydrogen assisted cracking of quenched and tempered high strength steels.

The presence of sufficiently concentrated hydrogen dissolved in the lattice just ahead of a crack tip aids whatever deformation processes the microstructure will allow. Intergranular, quasiclevage, or microvoid coalescence fracture modes operate depending on the microstructure, the crack tip stress intensity, and the concentration of hydrogen. The hydrogen does not hinder the motion of dislocations, but simply allows or forces the normal fracture processes to become operative at unusually low macroscopic strains, lowering the true fracture strength of the lattice. In the presence of a susceptible microstructure (which provides the crack tip and a stress concentration factor) and residual stress near the yield point, local lattice fracture strength is quickly overcome. The most susceptible microstructures in order of decreasing susceptibility are transformation twinned martensite, bainite characterized by large sheaves of narrow parallel ferrite laths, granular bainite, and finally the least susceptible; slipped martensite [Ref. 23]. The formation of martensite and the values of residual stresses present after welding are both dependent on the thermal cycling experienced during welding. The thermal gradient experienced during welding is dependent on the welding process, the plate thickness, and the temperature of the base metal [Ref. 24]. This gradient would increase as the temperature of the base metal decreases, resulting in more rapid cooling of the HAZ. This gradient causes a varying

cooling rate from the weld pool out to the base metal. The cooling rate in the as-cast weld metal and the unmixed, melted base metal region would be in effect a quench and the resulting microstructure would be dependent on the actual rate of cooling experienced [Ref. 25]. Ansell and Donachie [Ref. 26] examined the changes in the microstructure as a function of the quench rate. The morphology resulting from a slow quench is massive martensite characterized by packets of fine parallel laths containing a high dislocation density with very little retained austenite. When the quench rate is increased the width of the parallel lath martensite decreases. Increasing the quench rate also decreased the size of the Widmanstatten carbides present in the Fe-Ni-C alloy studied, while the thickness of any martensite twins which may have formed also decreased. It was noted that increasing the quench rate resulted in more martensite twins forming. In the areas of the weld that did not experience melting but were austenitized the cooling rate again produced fine lath martensite with similar characteristics to that described above. For the HAZ region not heated above the Al start temperature, the tempering effects on the low carbon martensite are the major consideration. Speich [Ref. 27] reported that 90% of the carbon segregates to dislocations and lath boundaries during cooling of low carbon martensite. Carbon segregation is very rapid in nickel alloyed iron because the diffusivity is increased 25 times the rate in pure gamma

iron. This information is in agreement with that reported by Ansell and Donachie [Ref. 28] where the carbon segregation acts as a nucleus for carbide growth. It was observed that during tempering at low temperatures (below 150° C) carbon segregation was occurring in the martensite but no carbides formed. A rod shape carbide precipitated when the tempering temperature was raised to 200° C--330° C. When tempering above 400° C, a spheroidal cementite (Fe_3C) carbide precipitates along the martensite laths and within the laths.

III. EXPERIMENTAL PROCEDURE

A. MACROSAMPLE PREPARATION

Two HY-80 steel plates, each measuring one inch thick, twelve inches long by eight inches wide were prepared by The Naval Ship Research and Development Center, Annapolis, Maryland. Each plate contained a weld joint running longitudinally. The joints were double beveled at 60 degrees and welded by standard shielded metal-arc welding procedures. One plate was preheated to 250° F (121° C) prior to welding and the other plate was cooled to 32° F (0° C). The cooled plate was to simulate winter welding conditions with no preheat. The interpass temperature was maintained at 32° F (0° C) by subsequent cooling between weld head passes.

Both welds were made using 11018, 3/16 inch (4.8 mm) alloy rod electrodes at a setting of 22 volts and 190 amperes. Rod composition and mechanical property limits are listed in Tables 4 and 5. The welding speed and heat input was 5-6 inches per minute (2.5 mm/sec) and 50 KJ/inch (2 KJ/mm) respectively. The plates were then sectioned perpendicular to the weld with a horizontal band saw into approximately one inch thick specimens. Each specimen face was cold sanded on a belt sander to produce a smooth, flat surface suitable for macroetching. A 2% nital solution was used to macroetch the samples and expose the weld characteristics of each

TABLE 4

CHEMICAL COMPOSITION LIMITS OF THE 11018
ALLOY ROD ELECTRODE (PERCENT)

ELEMENT	MIL-E-22200/1E 11018 Alloy Rod
Carbon	0.10 max.
Manganese	1.30--1.80
Silicon	0.60 max.
Phosphorus	0.030 max.
Sulfur	0.030 max.
Chromium	0.40 max.
Nickel	1.25--2.50
Molybdenum	0.25--0.50
Vanadium	0.05 max.
Water (covering)	0.20 max.
Iron	Remainder

TABLE 5

MECHANICAL PROPERTY LIMITS OF THE 11018 ALLOY ROD ELECTRODE

PROPERTY	MIL-E-22200/1E 11018 Alloy Rod
Tensile Strength (ksi)	100
Yield Strength 0.2% offset (ksi)	
As-welded	88/100
Stress Relieved	85
Elongation in 2 in. min. percent	
As-welded	20
Stress Relieved	20
Charpy V-notch min. impact (ft. lbs.)	
As-welded	20 @ -60° F
Stress Relieved	20 @ -60° F

sample. Each sample was submerged for 10 minutes until the details of each weld became evident. Figures 2 and 3 illustrate the prepared macrosamples of each weldment.

B. HARDNESS TESTING

Samples suitable for metallographic examination and comparison were selected from the last pass region of each specimen. Samples were cut and etched for five seconds after polishing in order to track the microhardness measurement locations, Figures 4 and 5. The locations with respect to the fusion line and visible heat affected zone were tabulated for each hardness measurement. Vickers microhardness measurements were made using a diamond indenter and a 200 gram load. Penetrations were made at 0.1 mm intervals along two linear traverses perpendicular to the visible fusion line.

C. METALLOGRAPHIC SAMPLE PREPARATION

After microhardness measurements were completed the samples were examined with a Zeiss Universal Photomicroscope. A series of photographs were taken along the microhardness traverse in an attempt to characterize and compare the microstructure present in each weld sample. Careful cataloguing was used to facilitate correlation of the microstructures with the associated Vicker's hardness. Each sample was then wafered along a plane parallel to the plane of the weld fusion zone using a low speed diamond wafering saw. Wafer

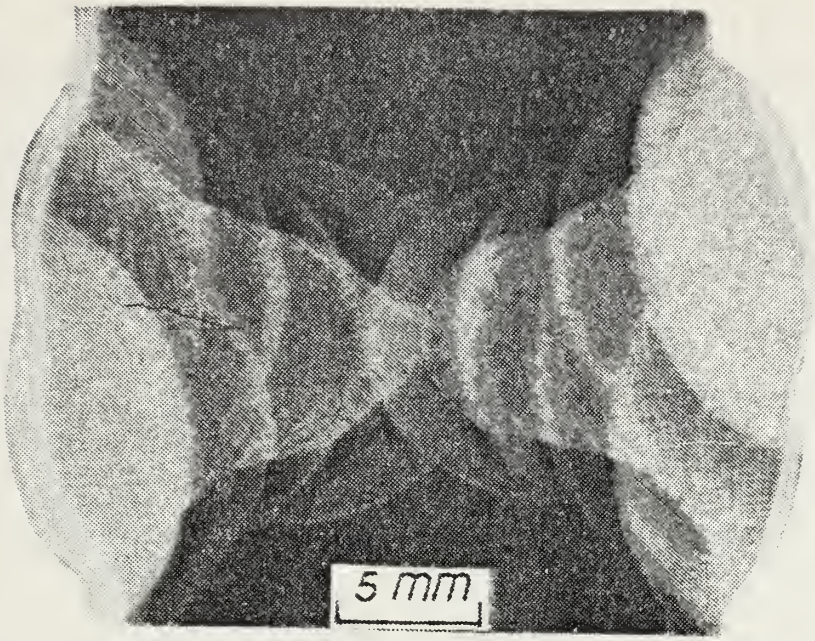

Figure 2. Macrosample of Preheated HY-80 Steel Weldment

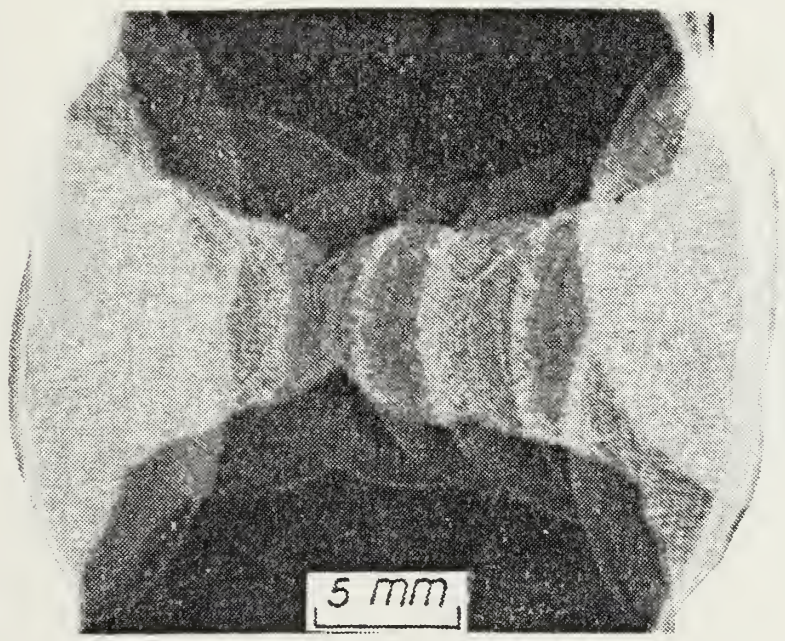

Figure 3. Macrosample of Non-Preheated HY-80 Steel Weldment

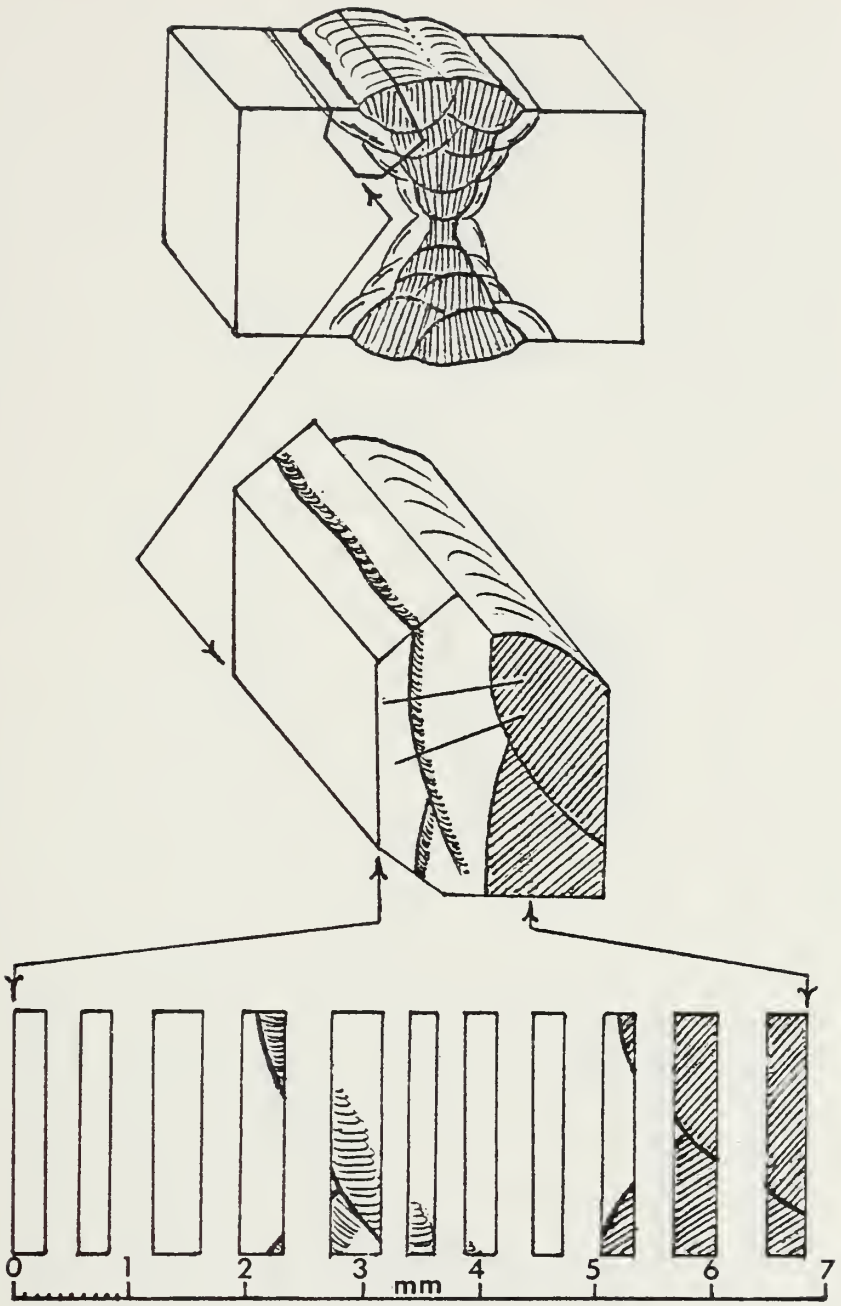

Figure 4. Wafer Cutting Locations From Preheated Weldment

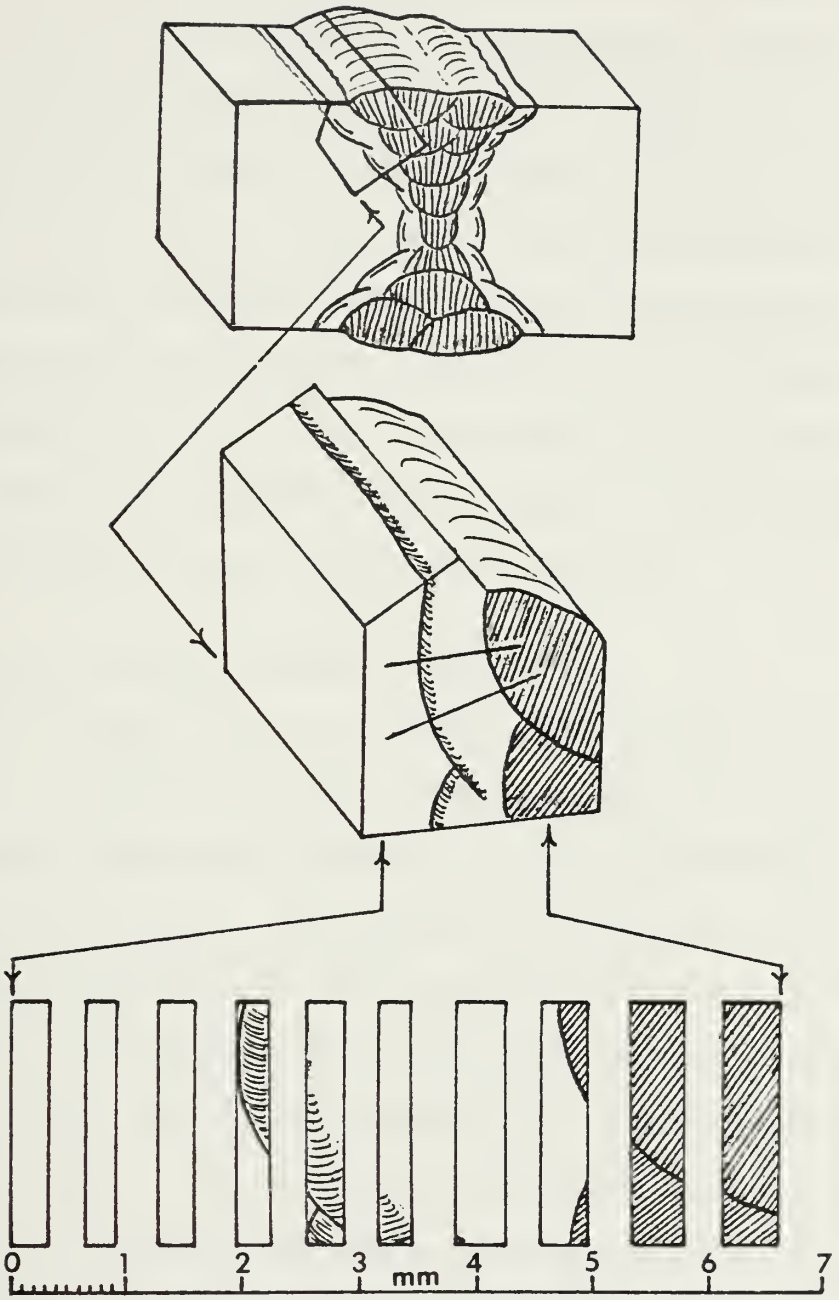

Figure 5. Wafer Cutting Locations From Non-Preheated Weldment

cutting locations are illustrated in Figures 4 and 5. Micrometer readings were taken of the sample prior to each cut and again after each cut to calculate the amount of material lost to the saw kerf and to precisely locate the wafer within the weldment. The physical locations of each wafer are listed in Tables 6 and 7. Each wafer was then mounted to a flat steel block using two sided adhesive tape for sanding and polishing using standard metallographic sample preparation techniques. The wafers were etched for eight seconds in a 2% nital solution and optical examination with the Zeiss was repeated on each sample to map the variations in microstructures within each specimen.

D. ELECTRON MICROSCOPY SAMPLE PREPARATION

A "whole" sample was cut perpendicular to the weld of each sample and prepared using standard metallographic techniques for conducting scanning electron microscopy. The SEM was used to better characterize the microstructure along the hardness traverse than was possible with the optical observations. The wafers previously prepared were also studied using the SEM to characterize the microstructure within each sample. Due to the three dimensional variations in each weld topography the exact location within each wafer used for selection of thin foil transmission electron microscopy samples was very critical. The three dimensional variations in each weld topography is illustrated in Figure 6. Microstructures from specific locations along the hardness

TABLE 6

WAFER LOCATIONS IN PREHEATED HY-80 STEEL WELDMENT

	Location				
	A	B	C	D	E
Distance from Fusion line (mm)	4.0	3.2	2.2	0.4	-0.4[a]

[a] Negative sign indicates inside fusion zone.

TABLE 7

WAFER LOCATIONS IN NON-PREHEATED HY-80 STEEL WELDMENT

	Location				
	A'	B'	C'	D'	E'
Distance from Fusion line (mm)	4.0	3.2	2.5	0.5	-0.4[a]

[a] Negative sign indicates inside fusion zone.

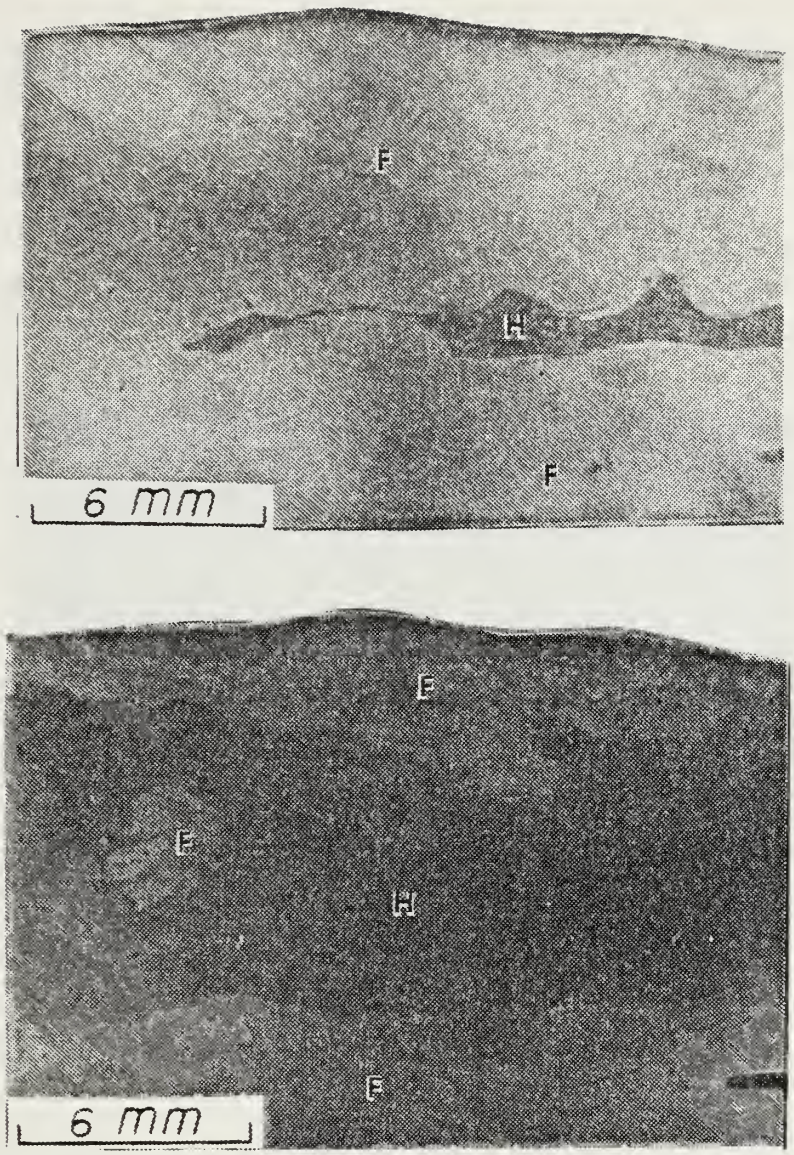

H - Heat Affected Zone

F - Fusion Zone

Figure 6. Three Dimensional Topography of HY-80 Steel Weldment

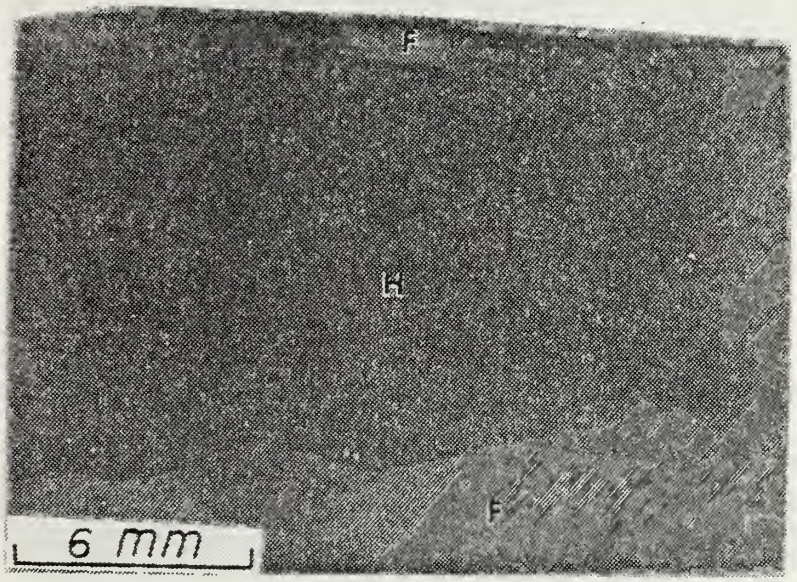

Figure 6. (Continued)

traverse as characterized by the "whole" sample SEM observations were matched with each wafer in similar physical locations within each weldment. Areas within each wafer that contained the desired microstructures were mapped so thin foil TEM samples could be prepared. This mapping allowed for the precise selection of each TEM thin foil sample and accurate correlation to its physical location within each weldment. Figure 7 shows an example of this matching of microstructures between the whole sample and a similarly located wafered sample.

Wafers selected for TEM study were thinned to 125 microns by hand sanding. Three-millimeter discs were punched out from the desired locations mapped previously. These discs were electropolished using a 10% perchloric acid, 90% methanol electrolyte cooled to approximately -45° C. Polishing was done at 16 volts and 50 milliamps using a Tenupol twin jet thinning apparatus. Transmission electron microscopy was utilized to characterize and compare the microstructures of each weld sample on a JEOL model JEM 120CX operating at 120 KeV.

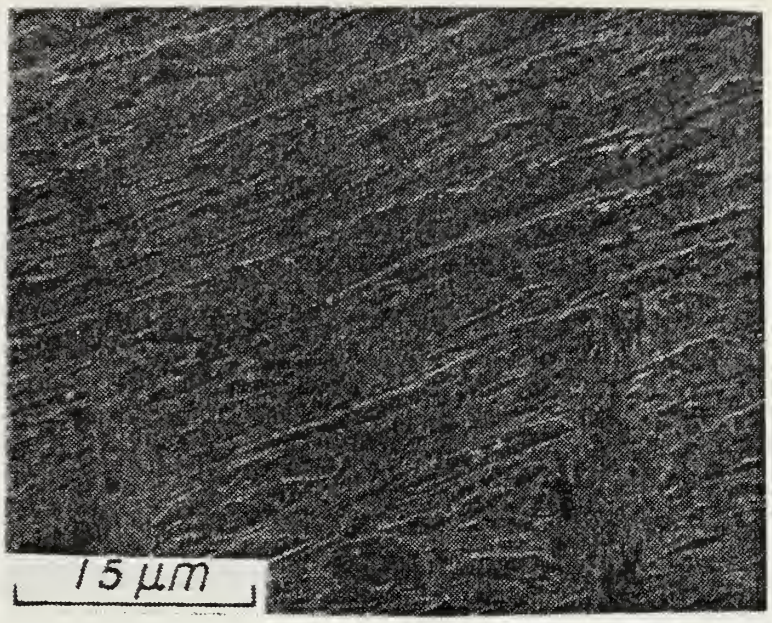

Whole Sample

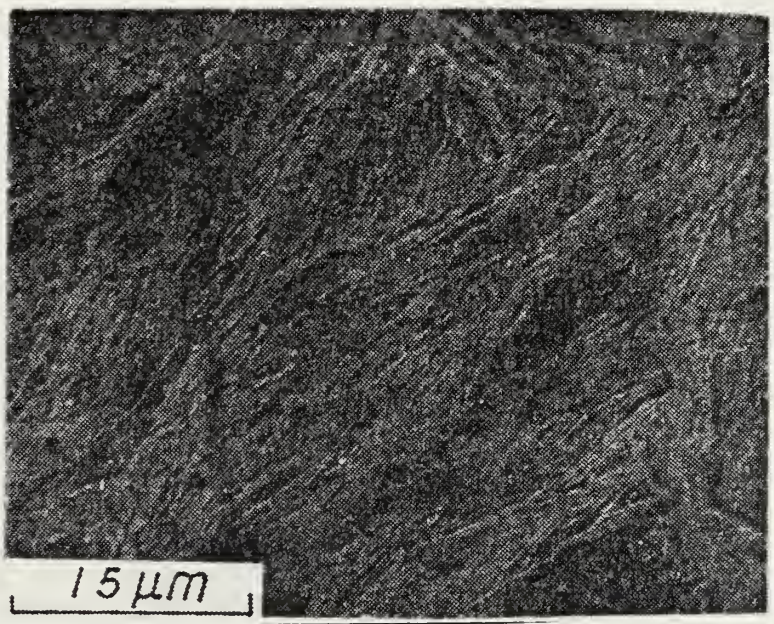

Selected Wafer

Figure 7. Microstructure Mapping for TEM Thin Foil Sample Selection

IV. EXPERIMENTAL RESULTS

A. HARDNESS MEASUREMENTS

The Vickers hardness traverse for each specimen was plotted and the results are illustrated in Figures 8 and 9. The hardness profile of the preheated specimen, Figure 8, shows a slight decrease from the parent base metal hardness value of 250 HV to 230 HV, as measurements approach the visible heat affected zone. Measurements crossing into the HAZ revealed a significant jump in the Vickers hardness, reaching peak hardness values of 430 HV. The hardness profile displays a two-tier plateau in the heat affected zone. The first plateau starts at the beginning of the visible HAZ, approximately 2.5 mm from the fusion line, and has an average hardness level of 420 HV. This first range of hardness values remain nearly constant 1.5 mm into the HAZ, where there is a slight decline. This retrogression to 412 HV marks the beginning of the second plateau which holds nearly constant hardness values across to the visible fusion line. The hardness then exhibits a steep decline in values to approximately 325 HV just inside the visible fusion zone. The hardness of the as-cast weld metal then tails off slightly to nearly match the hardness of the parent base metal. Five distinct regions characterized by these hardness trends were selected for further investigation. The regions, labeled A through E, are listed below and illustrated in Figure 8.

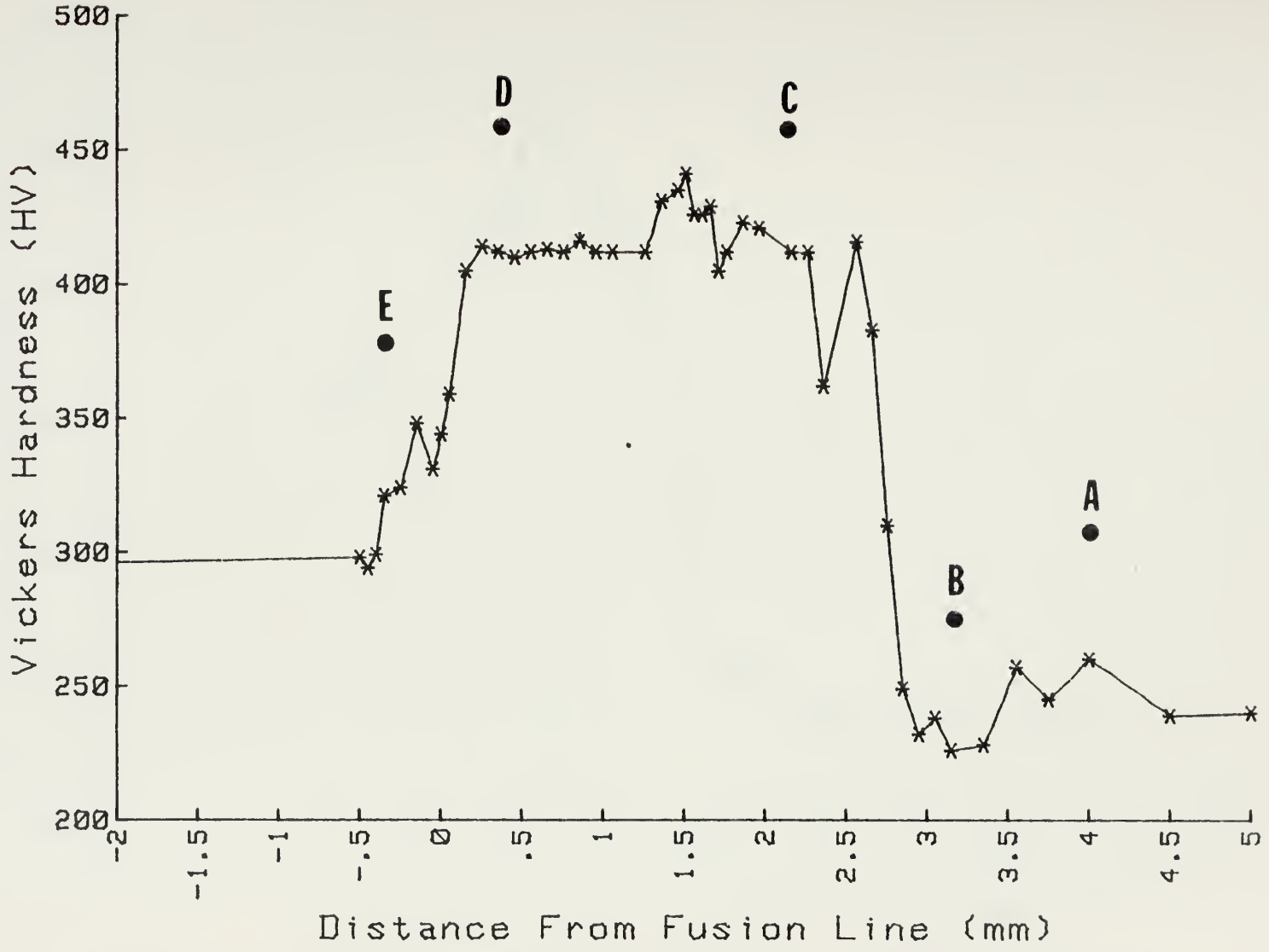

Figure 8a. Vickers Hardness Traverse of Preheated Weldment

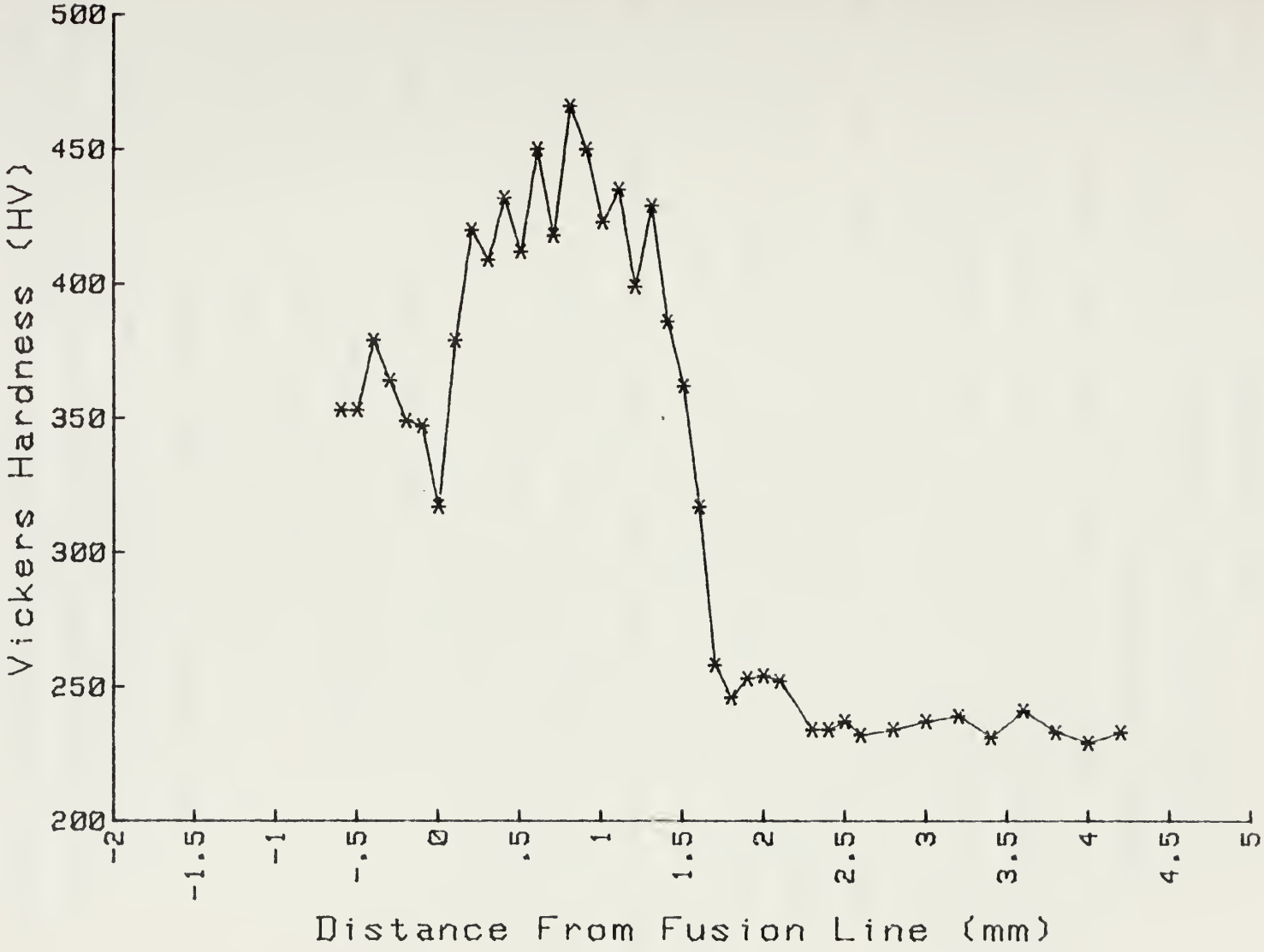

Figure 8b. Vickers Hardness Traverse of Preheated Weldment

Location A: Parent Base Metal

Location B: Overtempered Base Metal Region

Location C: Grain Refined Region

Location D: Chain Coarsened Region

Location E: Alloying Region of the Fusion Zone.

The hardness profile of the non-preheated specimen, Figure 9, shows a base metal hardness of 225 HV. There is a slight softening to 220 HV as the traverse approaches the visible heat affected zone. The HAZ has a radical fluctuation in the hardness with a continually increasing trend and a peak value of 410 HV near the visible fusion line. The hardness across the visible fusion line drops sharply to a value of 280 HV and slowly declines in the as-cast weld metal to nearly match the parent base metal. For comparison purposes the locations selected for further investigation in the non-preheated specimen correspond to the five locations chosen in the preheated sample. The locations A' through E' are listed below and illustrated in Figure 9.

Location A': Parent Base Metal

Location B': Overtempered Base Metal Region

Location C': Grain Refined Region

Location D': Grain Coarsened Region

Location E': Alloying Region of the Fusion Zone.

Additional hardness traverses from identical weld regions in the preheated and non-preheated samples were completed to confirm the differences in hardness measures

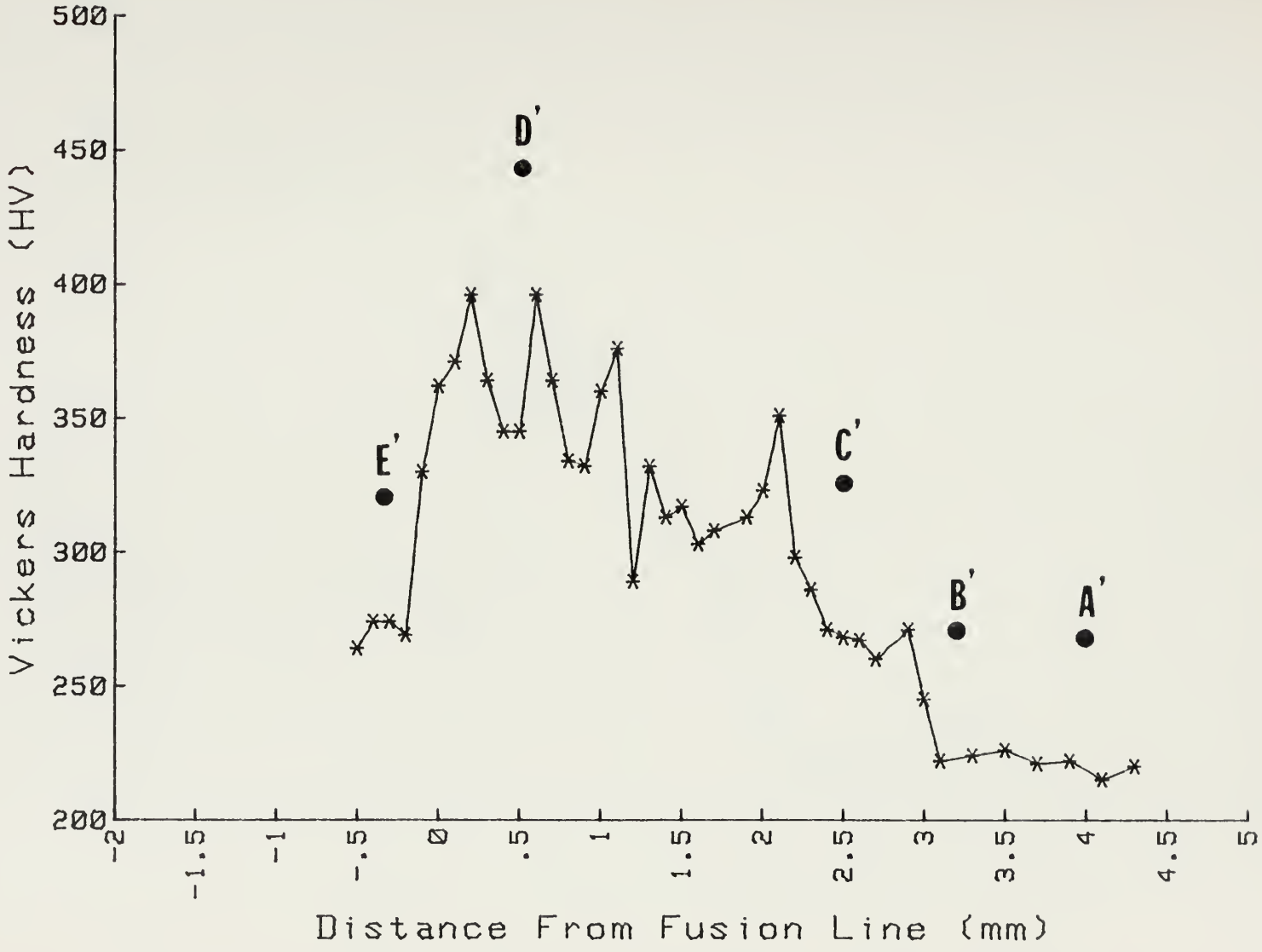

Figure 9a. Vickers Hardness Traverse of Non-Preheated Weldment

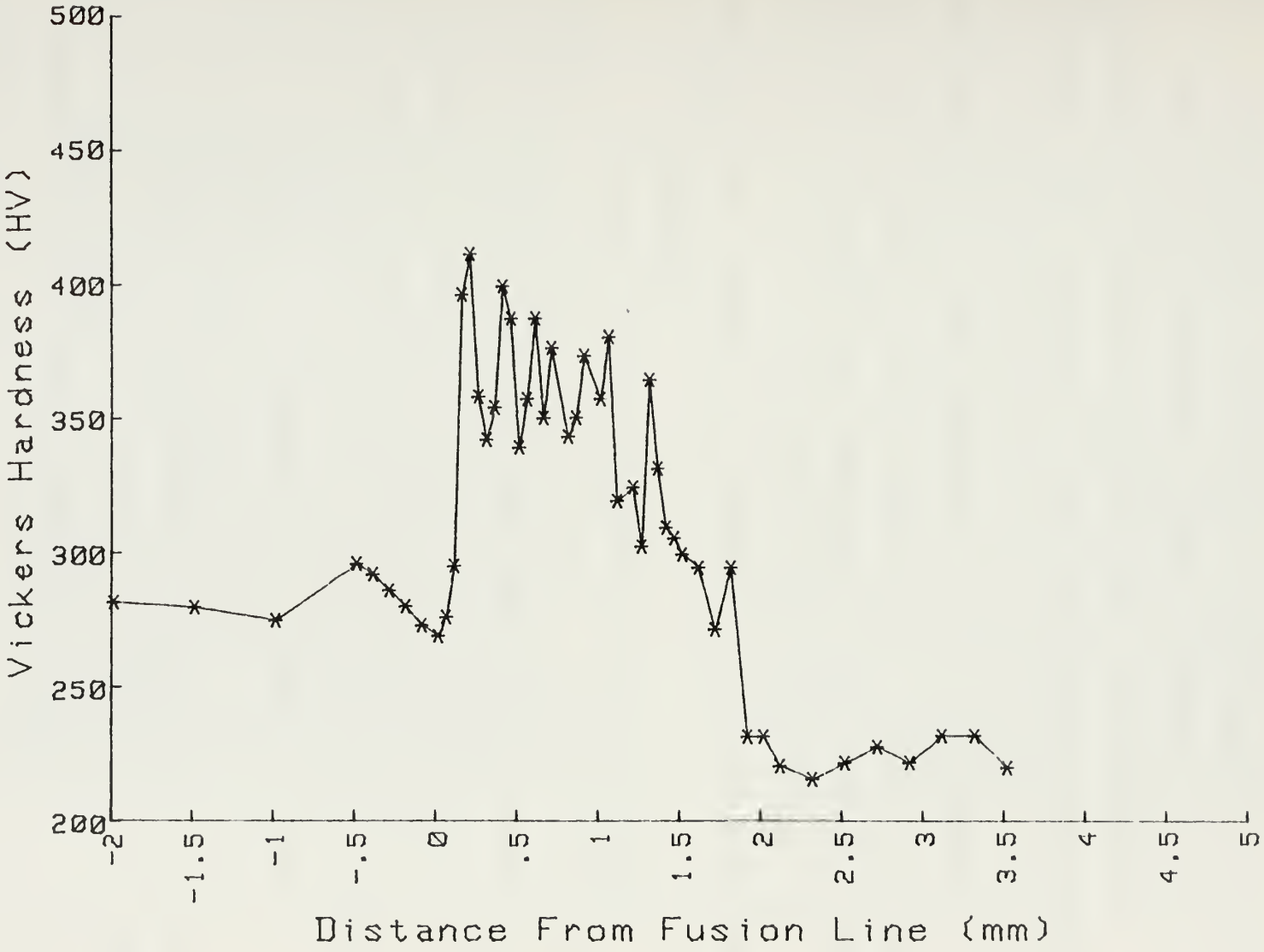

Figure 9b. Vickers Hardness Traverse of Non-Preheated Weldment

were due to preheating, not underlying weld passes, Figures 8b and 9b.

B. MICROSTRUCTURAL OBSERVATIONS IN THE PREHEATED WELDMENT

The preheated weldment, Regions A through E, were examined with optical, scanning electron (SEM), and transmission electron (TEM) microscopy. This investigation was conducted to gain an understanding of, and to characterize, the microstructures in the heat affected zone of a shielded metal arc (SMA) weldment in HY-80 steel plate. Optical and scanning electron microscopy were conducted on cross sectional areas of the weld and its heat affected zone representing the same locations examined by transmission electron microscopy.

1. Location A

Location A is the designation given to the base metal area selected for investigation. Optical investigation revealed little information other than a fine microstructure throughout the base metal, Figure 10. The microstructure as observed by scanning electron microscopy at 2000X, revealed a martensitic structure within visible prior austenite grain boundaries. A dispersion of carbides is visible throughout the microstructure, Figure 11. The microstructure in Location A, characterized by transmission electron microscopy, is that of a mixture of a tempered bainite and tempered martensite duplex structure. Figure 12(a) shows typical tempered bainitic and martensitic regions found in

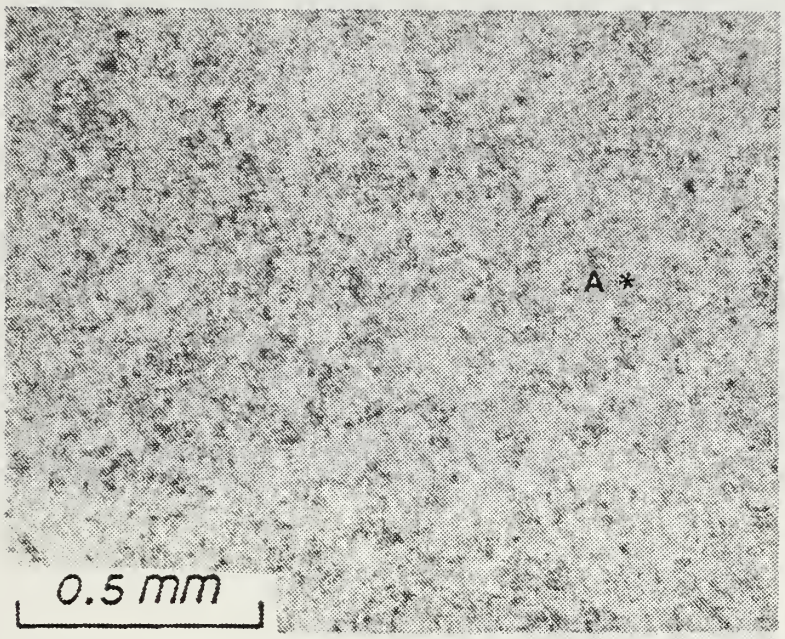

Figure 10. Optical Micrograph of Location A

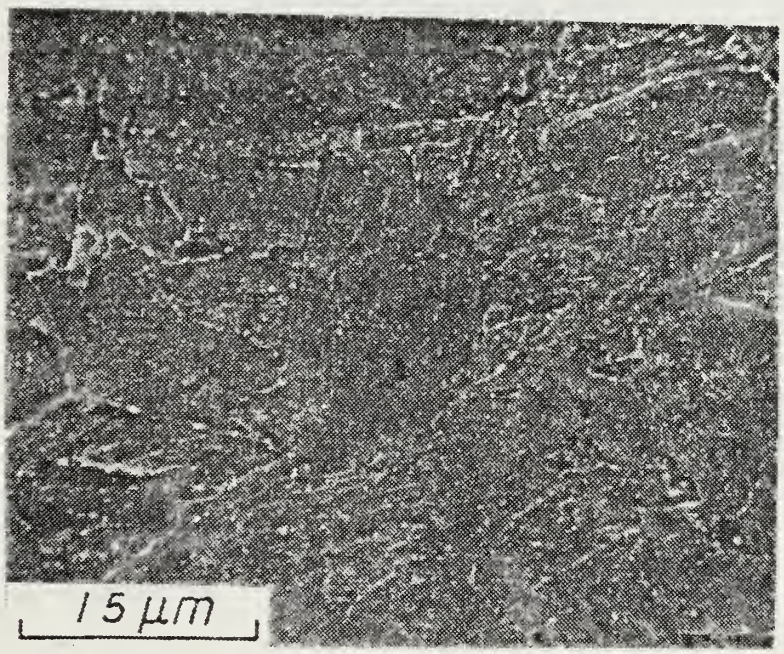

Figure 11. SEM Micrograph of Location A

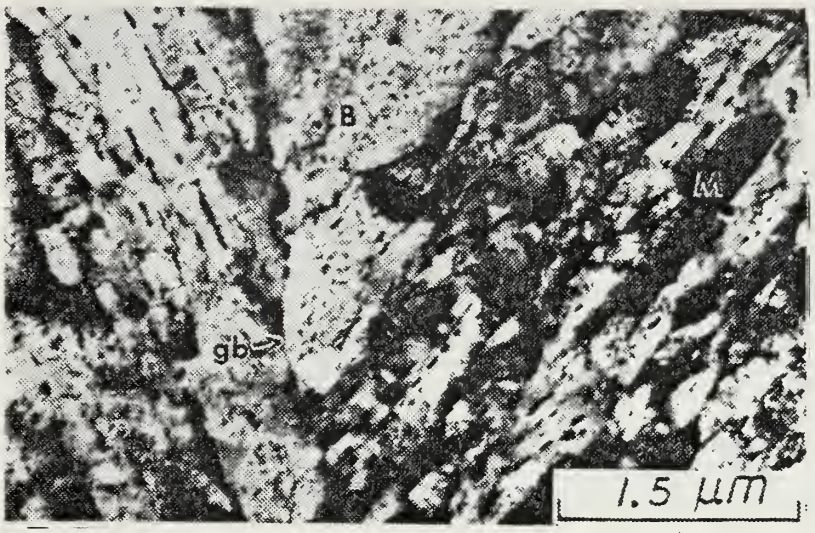

(a)

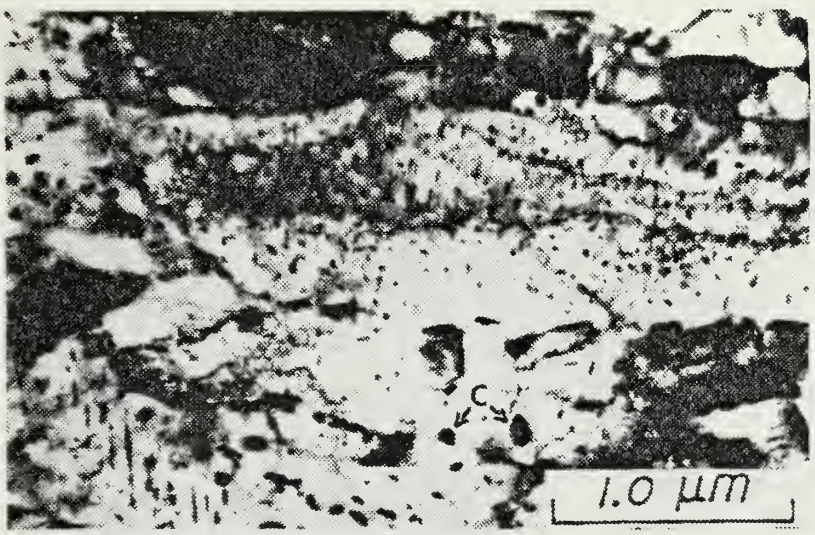

(b)

Tempered Martensite = (M)
Tempered Bainite = (B)
Temper Carbides = (C)
Prior Austenite
Grain Boundary = (gb)

Figure 12. TEM Micrographs of Location A

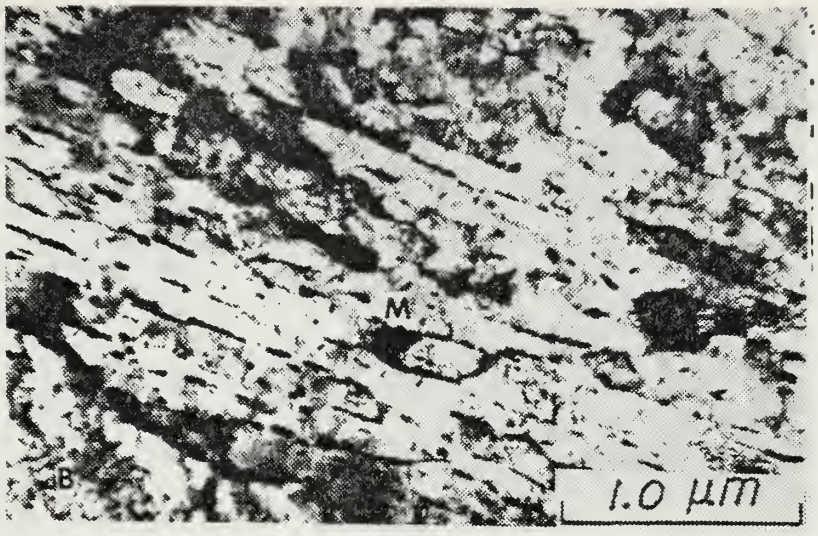

(c)

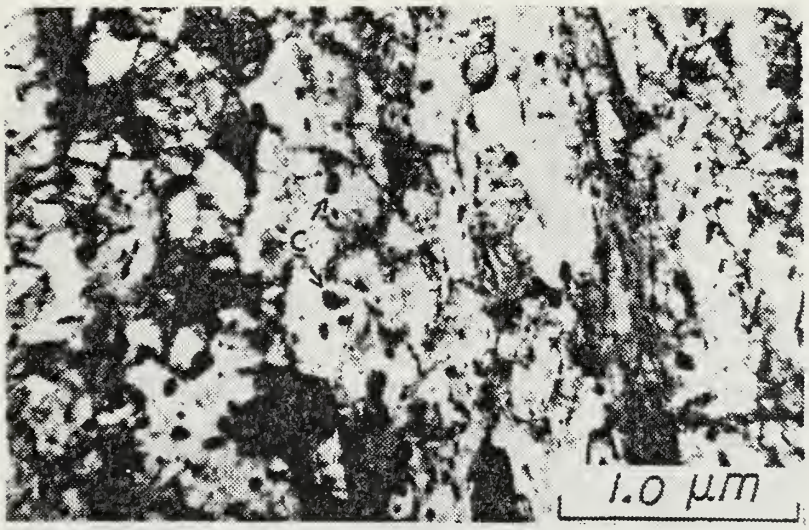

(d)

Figure 12. (CONTINUED)

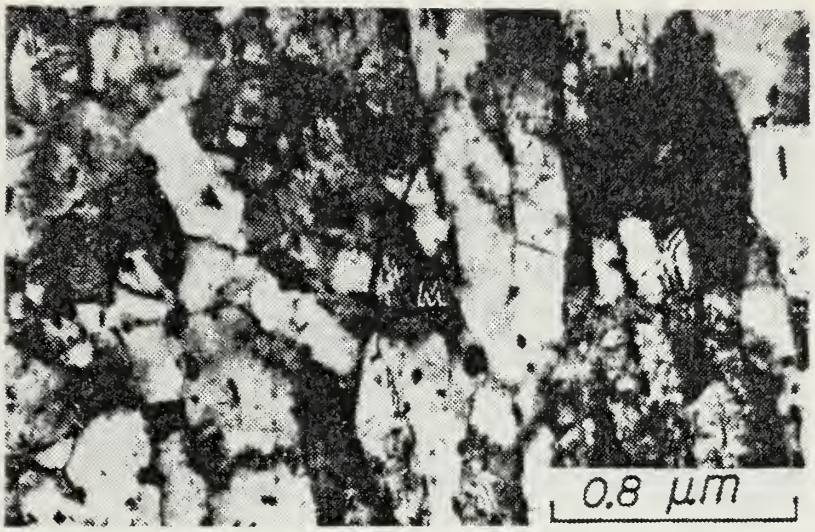

(e)

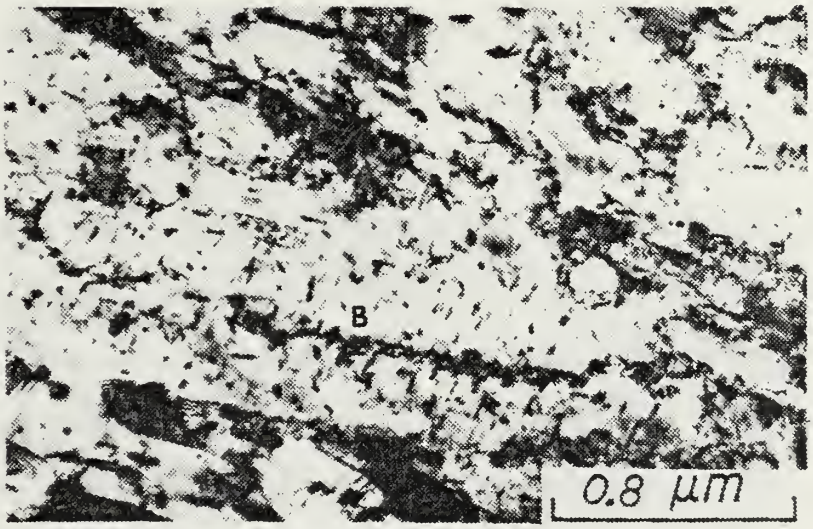

(f)

Figure 12. (CONTINUED)

the as-heat treated material with a prior austenite grain boundary decorated with coarse carbides. There is a uniform distribution of cementite (Fe_3C) particles with average diameters of about 0.08 microns within the laths and on the austenite grain boundaries, Figure 12(a-f). The average martensite lath width is about 0.4 microns while the bainite lath average is about one micron.

2. Location B

Location B is in the region of slightly depressed hardness near the visible heat affected zone approximately 3.2 millimeters from the fusion line. The microstructure as seen with optical and scanning electron microscopy in "B" appears to be very similar to that within "A", Figures 13 and 14. Examination of the specimen in Location B by transmission electron microscopy reveals a microstructure consisting of tempered bainite and tempered martensite with uniform distribution of cementite. These spherical cementite particles are approximately the same size as those observed in A. The cementite in A are still present in B. The martensite and bainite average lath sizes are about 0.3 and 0.5 microns respectively. Figure 15(a-f) illustrates the typical microstructures found in Location B.

3. Location C

Location C is in the grain refined heat affected zone as shown in Figure 16. Optical investigation shows a significant reduction in the grain size which produces a visible

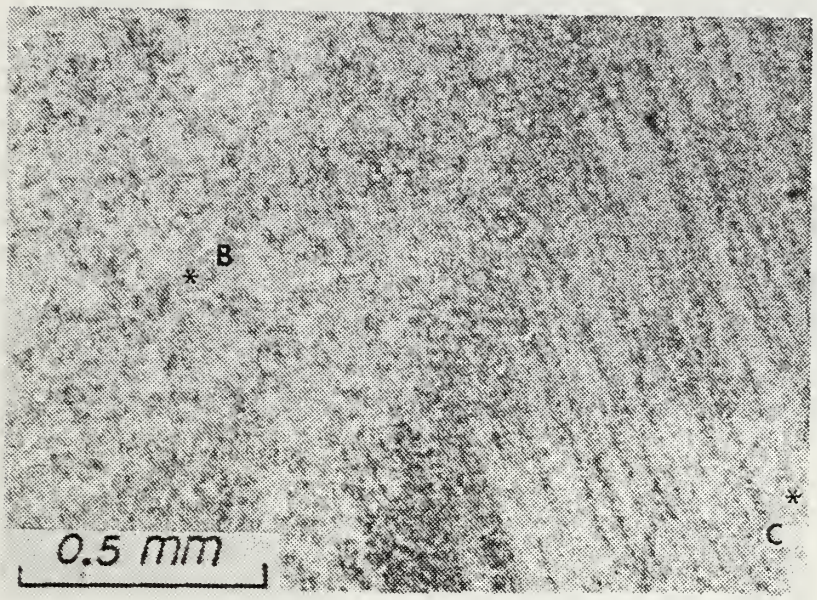

Figure 13. Optical Micrograph of Location B

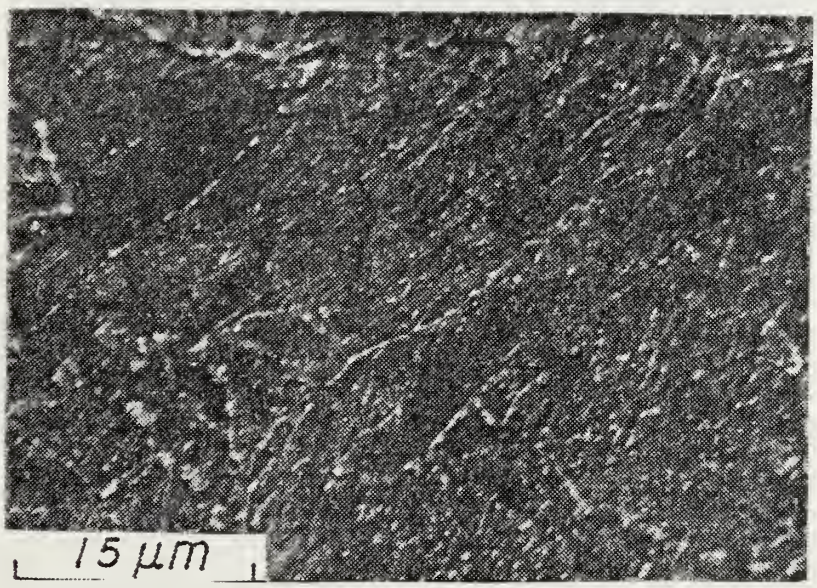

Figure 14. SEM Micrograph of Location B

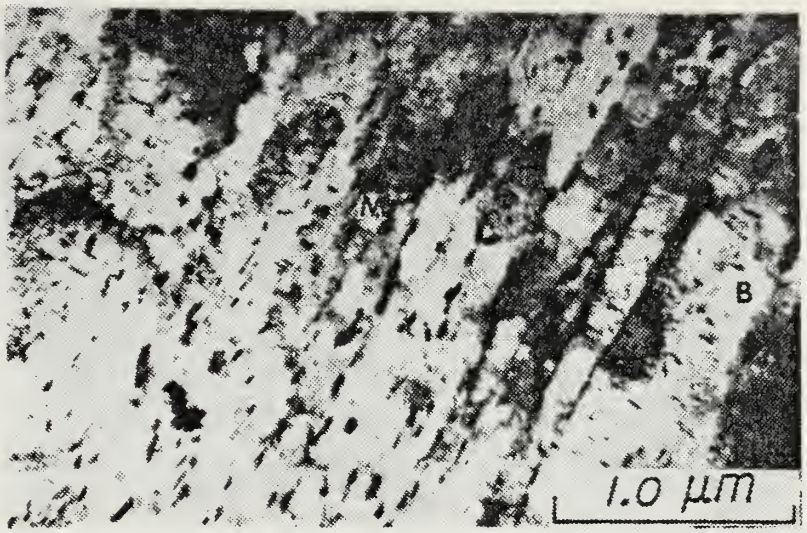

(a)

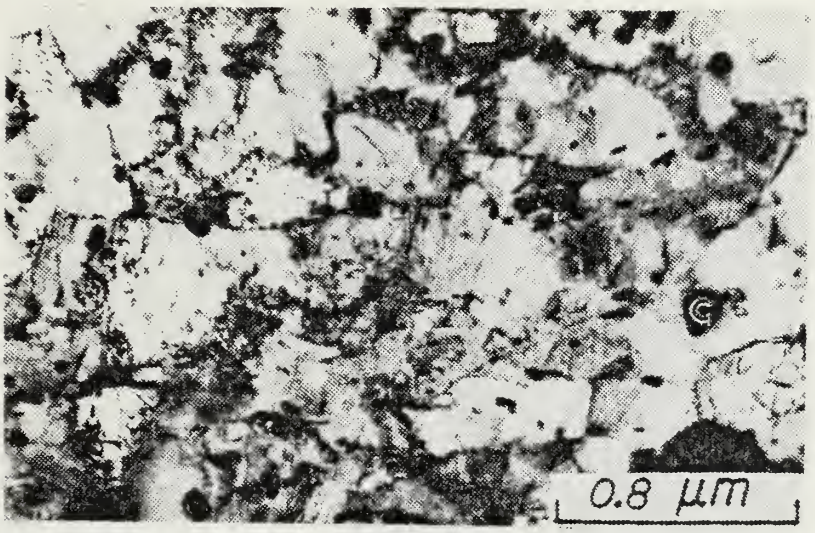

(b)

Tempered Martensite = (M)
Tempered Bainite = (B)
Temper Carbides = (C)
Prior Austenite
Gain Boundary = (gb)

Figure 15. TEM Micrographs of Location B

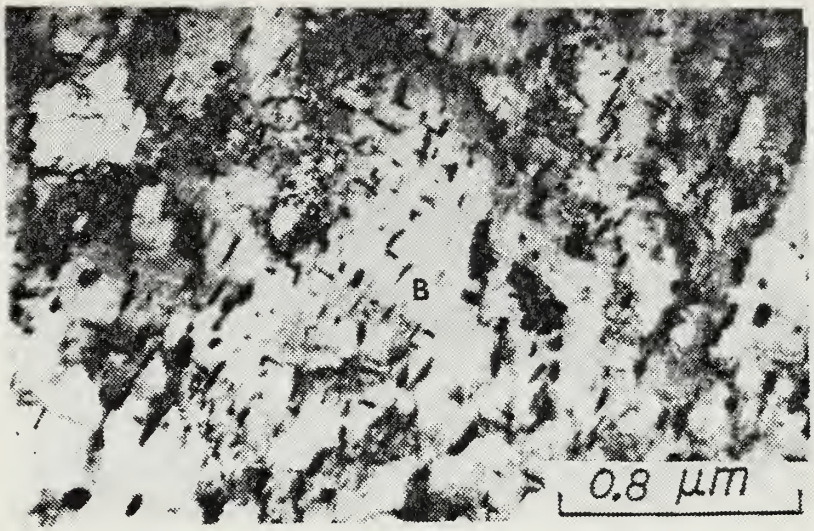

(c)

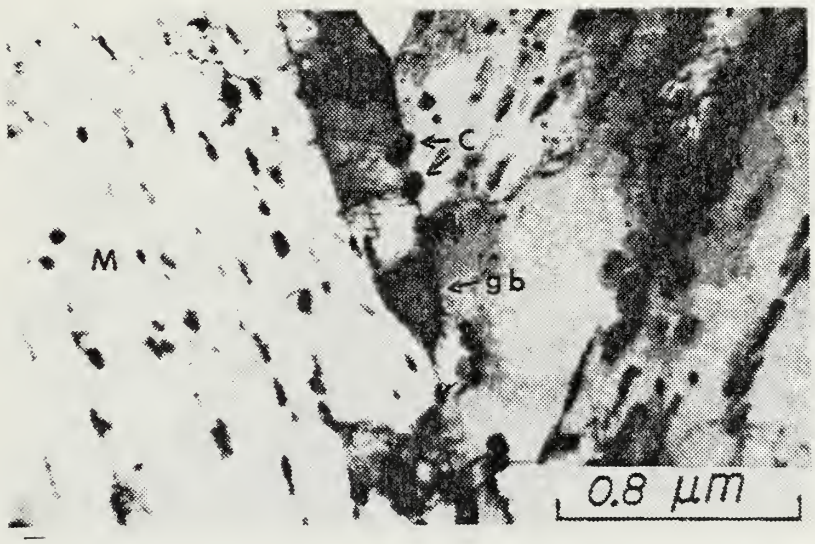

(d)

Figure 15. (CONTINUED)

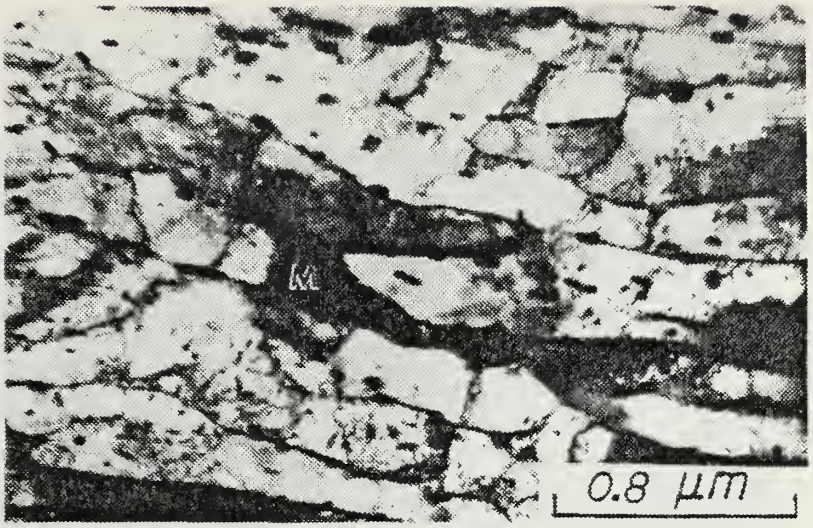

(e)

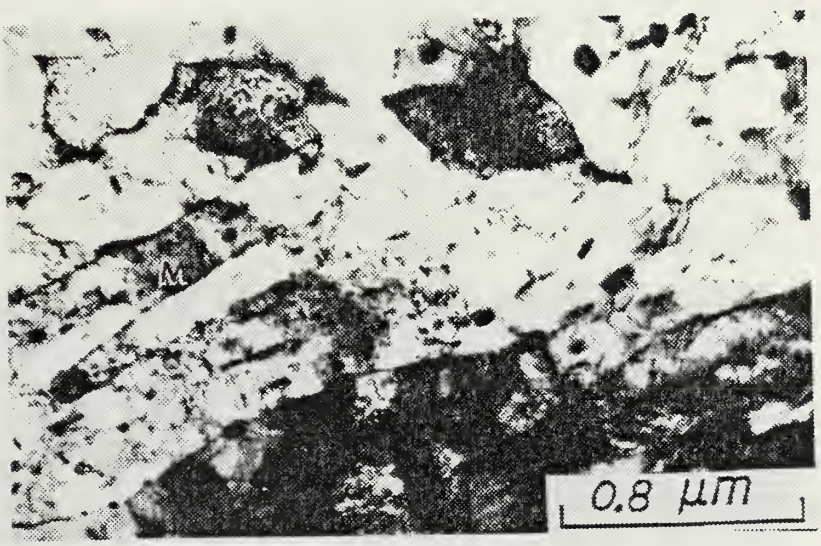

(f)

Figure 15. (CONTINUED)

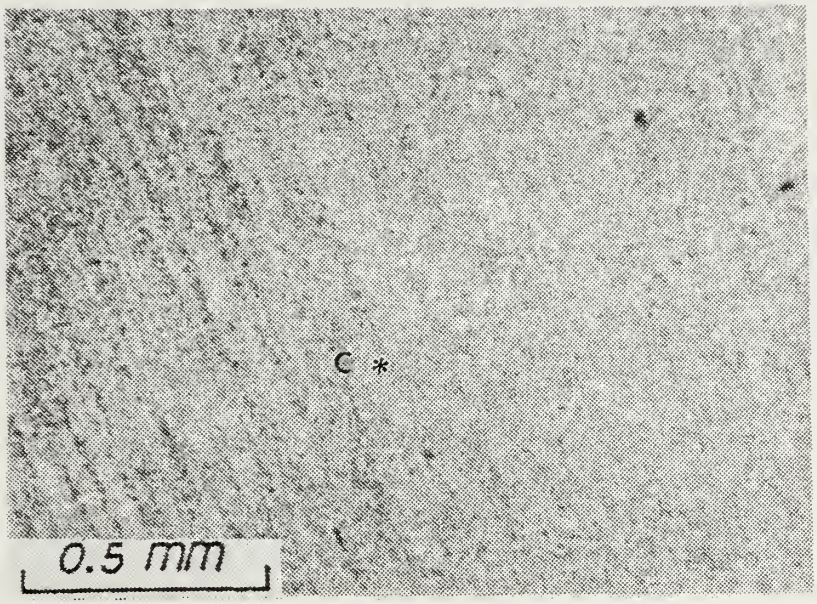

Figure 16. Optical Micrograph of Location C

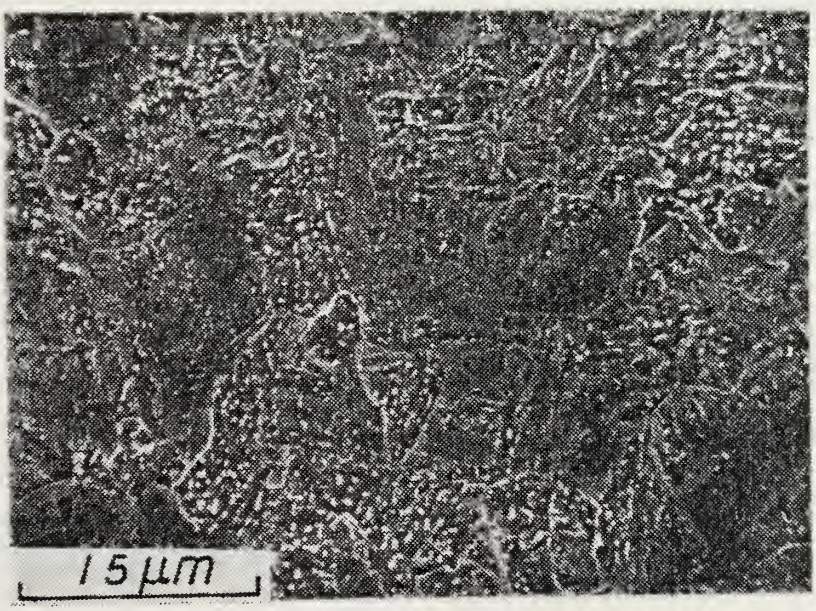

Figure 17. SEM Micrograph of Location C

demarcation between the heat affected zone and the base metal. SEM micrographs at 2000X reveal a mixed martensitic structure of newly transformed and the original tempered martensite with coarse carbides remaining in the original martensite, Figure 17. TEM examination revealed three distinctly different structures; fine lath, heavily dislocated martensite, autotempered martensite and the original tempered structure, Figures 18(a-f). The average lath width of the heavily dislocated martensite is about 0.2 microns and the original tempered microstructure has a lath width unchanged, i.e., similar to "A" and "B".

4. Location D

Location D is the grain coarsened heat affected zone near the visible fusion line. Optical investigation clearly reveals the significant increase in grain size, Figure 19. The microstructure appears to be martensite, which is more easily recognized in Figure 20, a scanning electron micrograph at 2000X. The TEM specimens exhibit a heavily dislocated fine lath martensite (0.2 microns average) mixed with a coarser autotempered martensite (0.8 microns average). The spherodized carbides present in "A", "B" and "C" are no longer visible within the microstructure of D indicating complete austenization and dissolution of the temper carbides. The presence of a transformation twinned martensite within the coarse ferrite laths was observed but very infrequently, Figures 21(a-f).

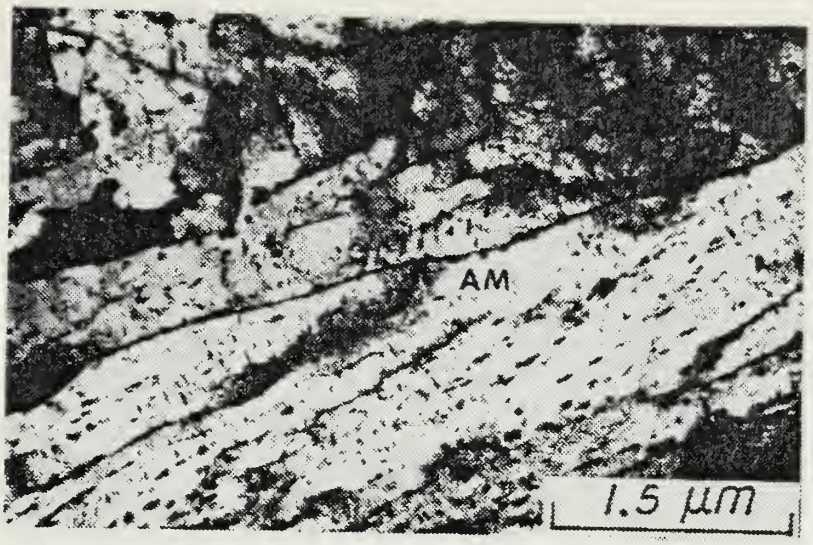

(a)

Autotempered Martensite (AM)

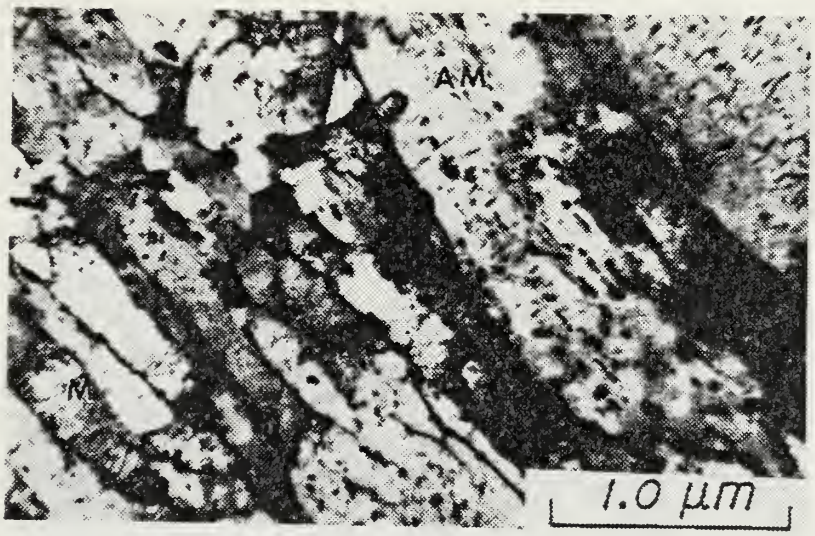

(b)

Original Tempered Microstructure (M)
New Autotempered Martensite (AM)

Figure 18. TEM Micrographs of Location C

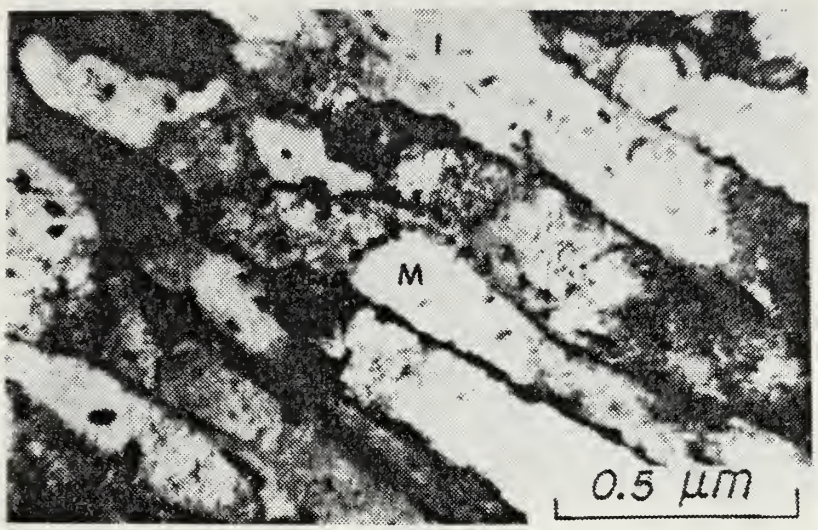

(c)

Original Tempered Microstructure

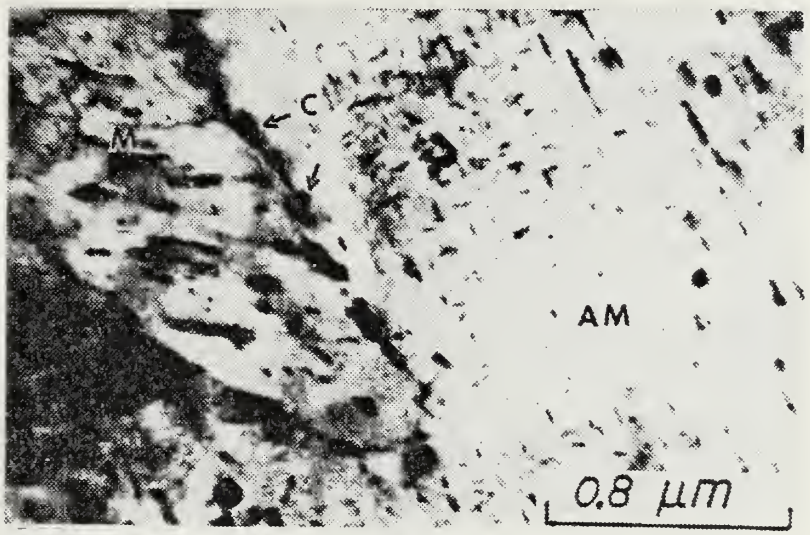

(d)

Original Tempered Microstructure
New Autotempered Martensite (AM)
Temper Carbides (C)

Figure 18. (CONTINUED)

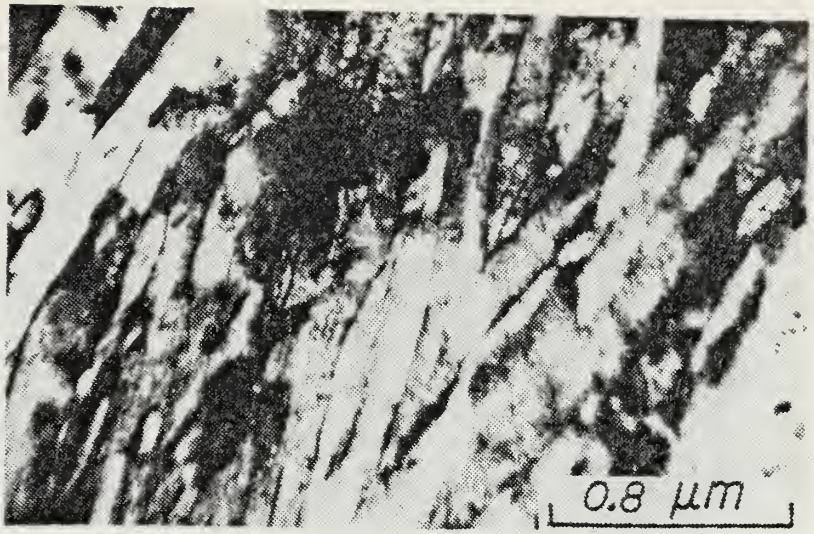

(e)

Newly Transformed Martensite

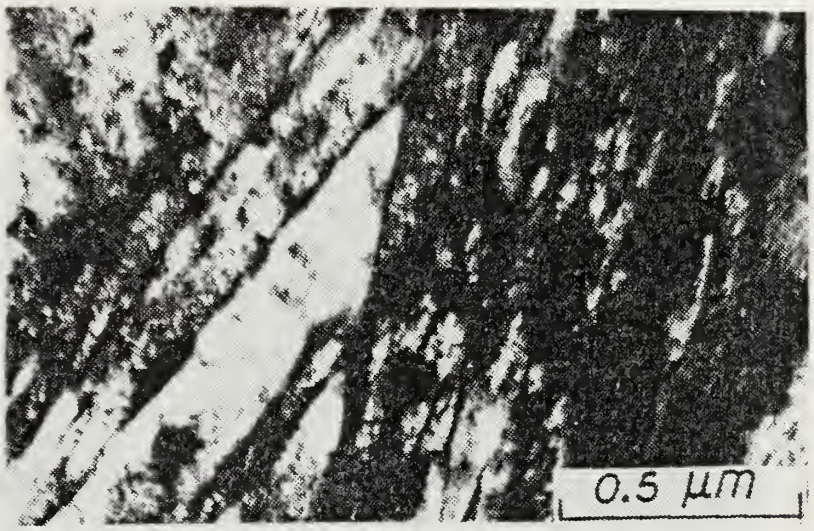

(f)

Newly Transformed Martensite

Figure 18. (CONTINUED)

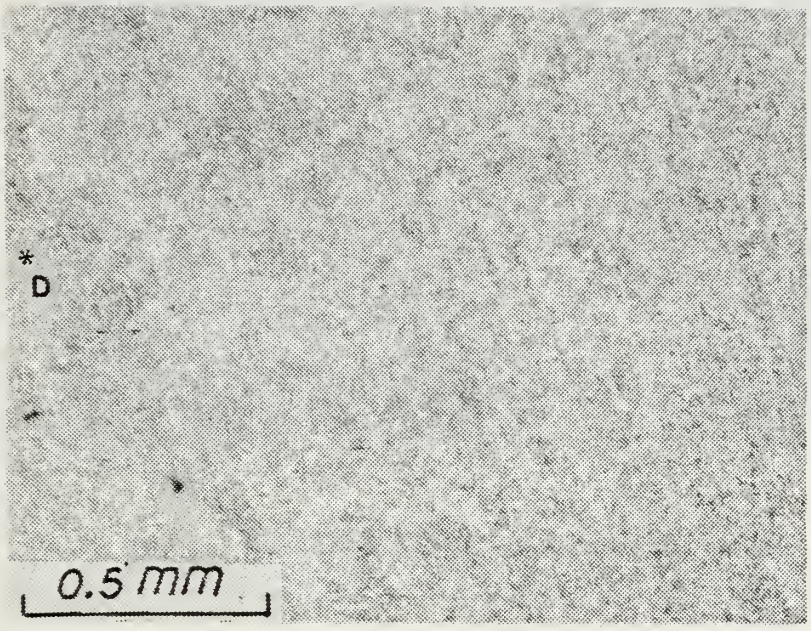

Figure 19. Optical Micrograph of Location D

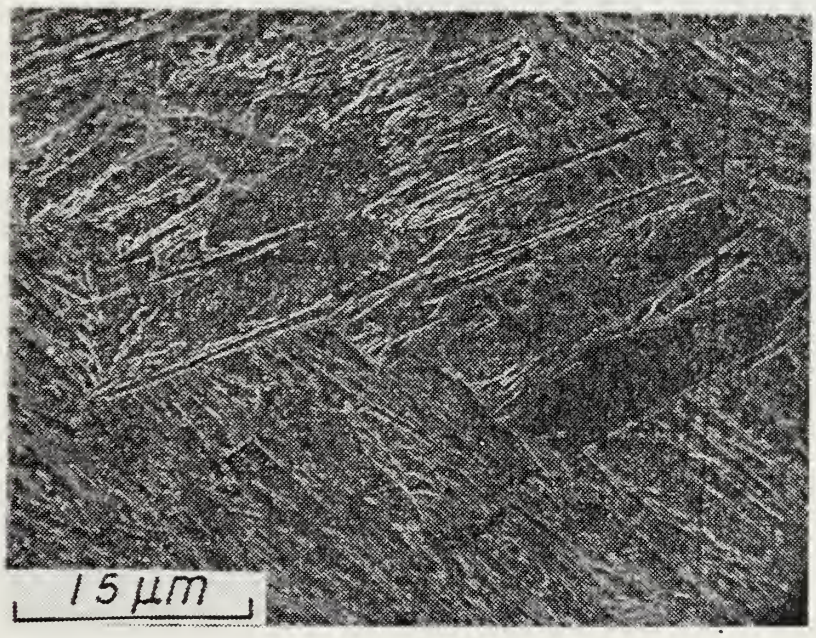

Figure 20. SEM Micrograph of Location D

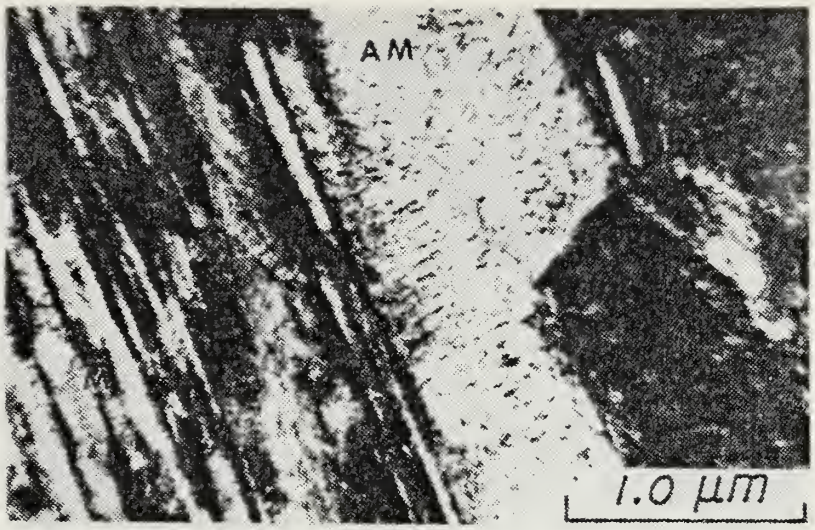

(a)

Autotempered Martensite (AM)

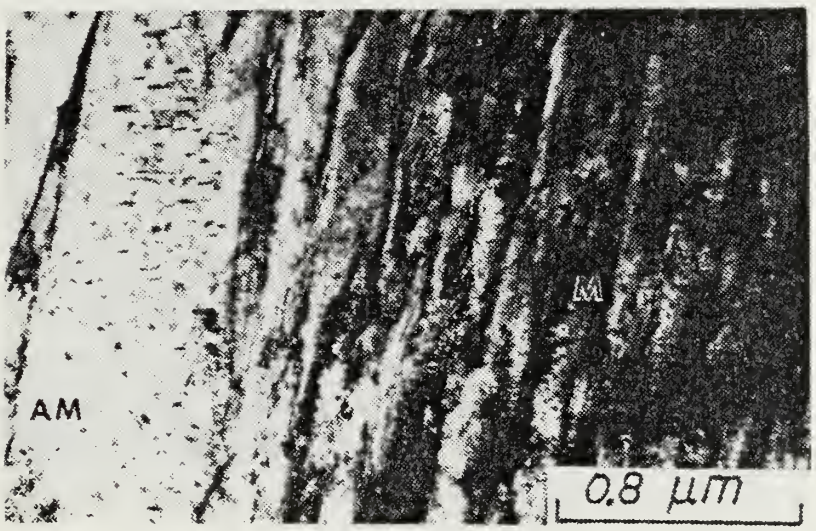

(b)

Figure 21. TEM Micrographs of Location D

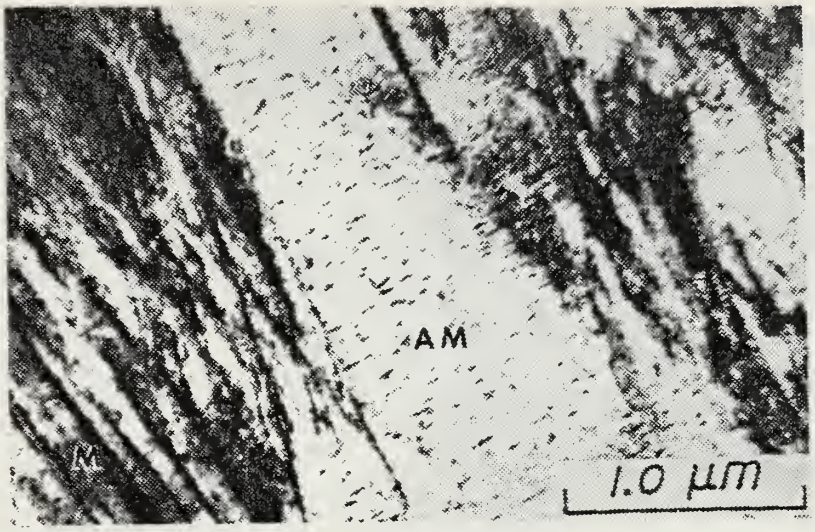

(c)

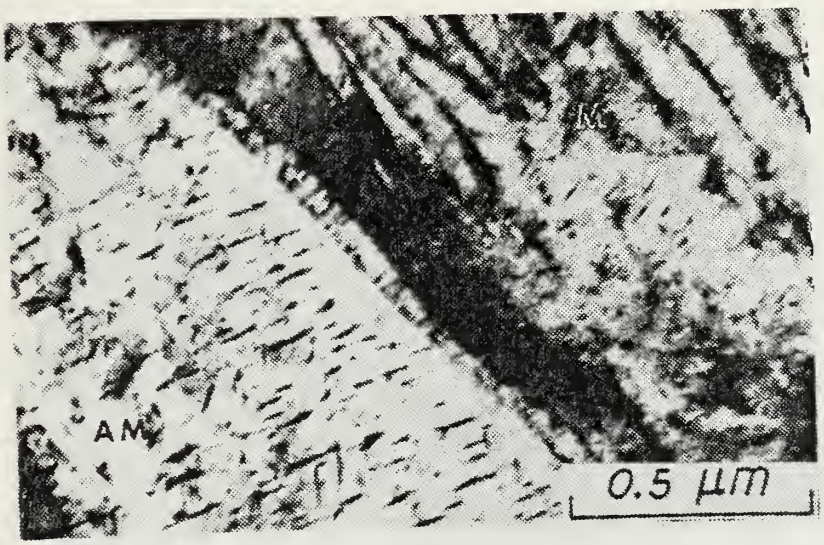

(d)

Figure 21. (CONTINUED)

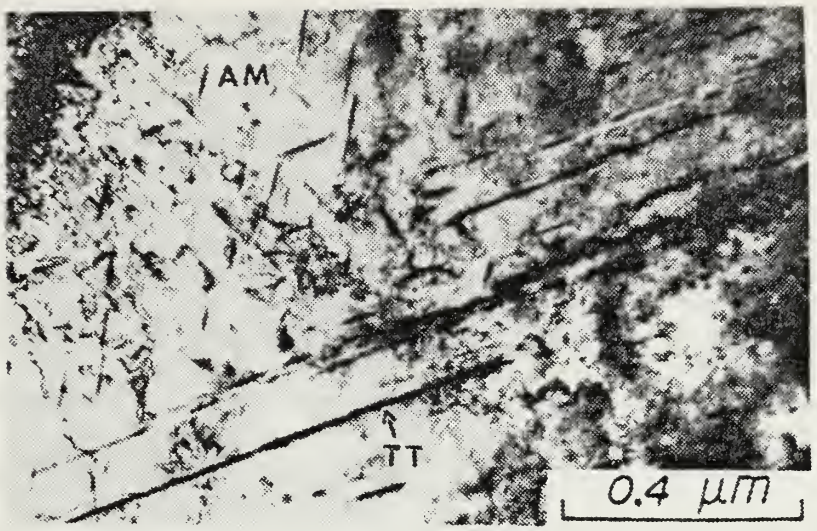

(e)

Transformation Twinned Martensite (TT)

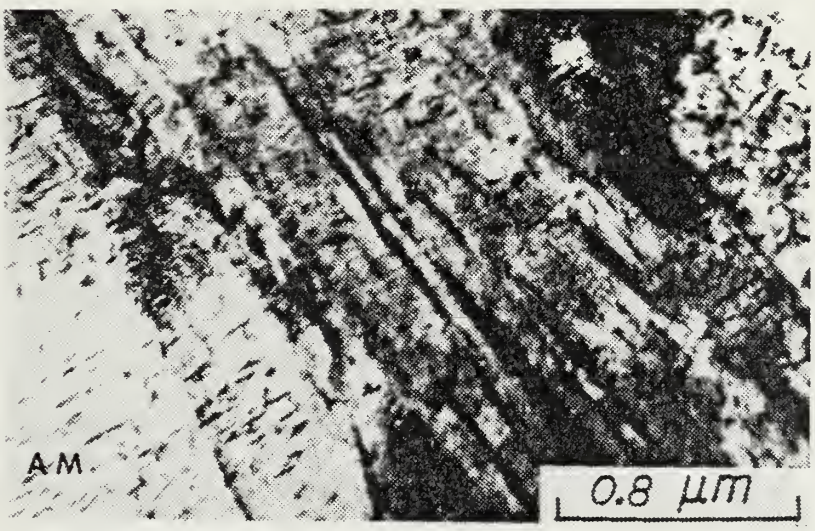

(f)

Figure 21. (CONTINUED)

5. Location E

The as-cast weld metal near the visible fusion line (alloying region) is designated Location E. The optical micrograph, Figure 22, clearly shows a significant change in the microstructure. However low magnification observation fails to reveal any specific information regarding the characteristics of the weld microstructure. Scanning electron microscopy, Figure 23, displays a coarse lath martensitic structure within the prior austenite grains. The transmission electron microscope confirms that the bulk of the microstructure is made up of a low carbon lath martensite. The average lath width was determined to be 0.3 microns. There were small amounts of retained austenite coating many of the lath interfaces, and a trace of twinning was located within a few martensite laths, Figures 24(a-f).

C. MICROSTRUCTURAL OBSERVATIONS IN THE NON-PREHEATED WELDMENT

The non-preheated weldment, Locations A' through E' were examined by the same techniques utilized for the preheated specimen. The microstructure in the heat affected zone was examined for characterization and comparison with that of the preheated HY-80 weldment.

1. Location A'

Location A' is in the area of the non-preheated base metal. The microstructures observed were the same as found in A, Figures 10, 11 and 12(a-f).

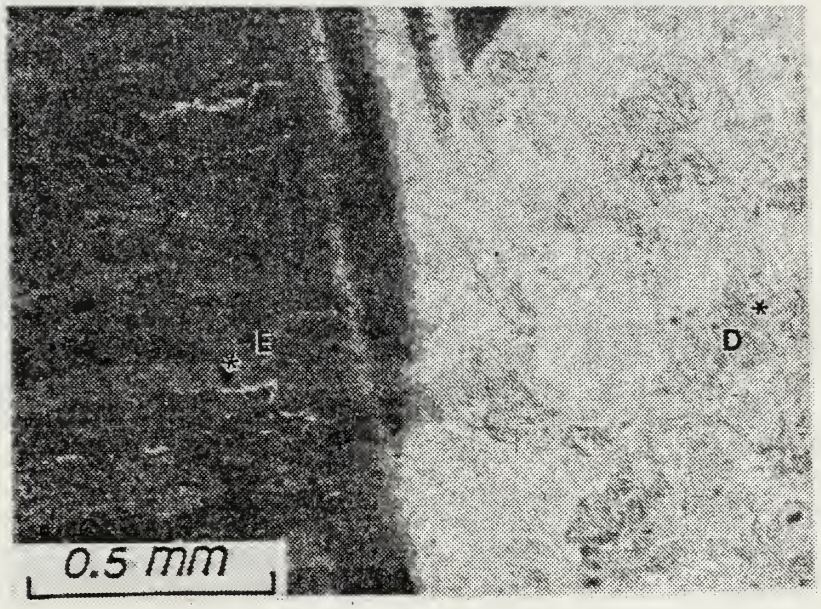

Figure 22. Optical Micrograph of Location E

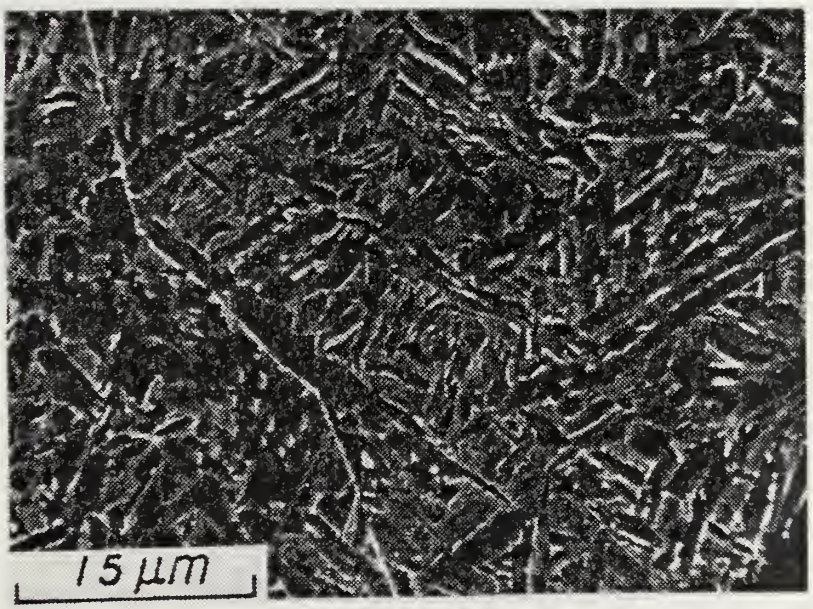

Figure 23. SEM Micrograph of Location E

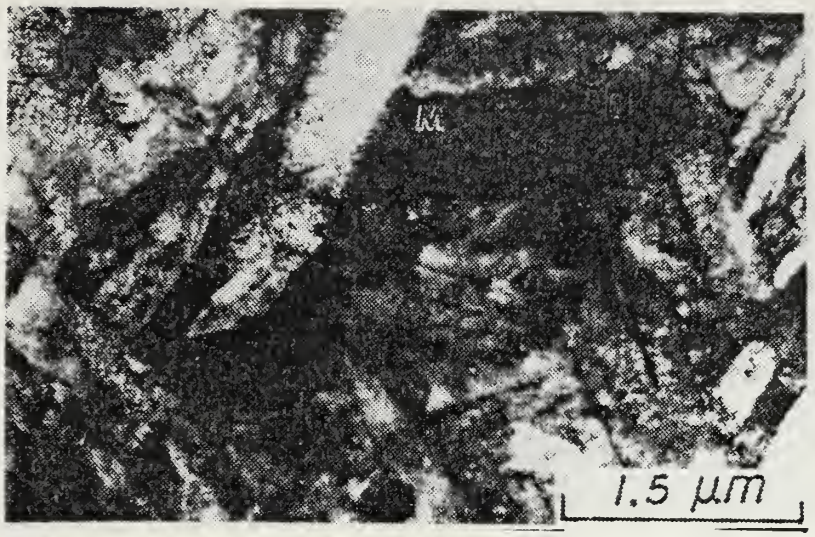

(a)

(b)

Figure 24. TEM Micrographs of Location E

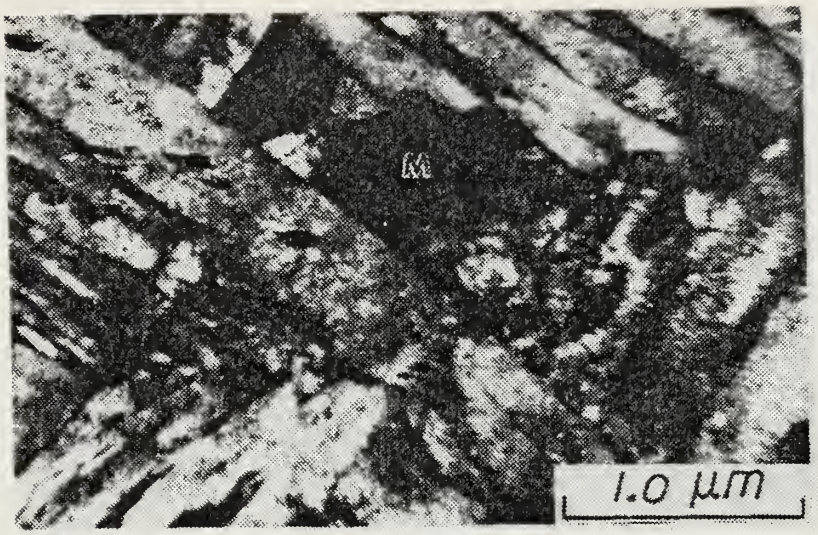

(c)

(d)

Retained Austenite (A)

Figure 24. (CONTINUED)

(e)

Retained Austenite (A)

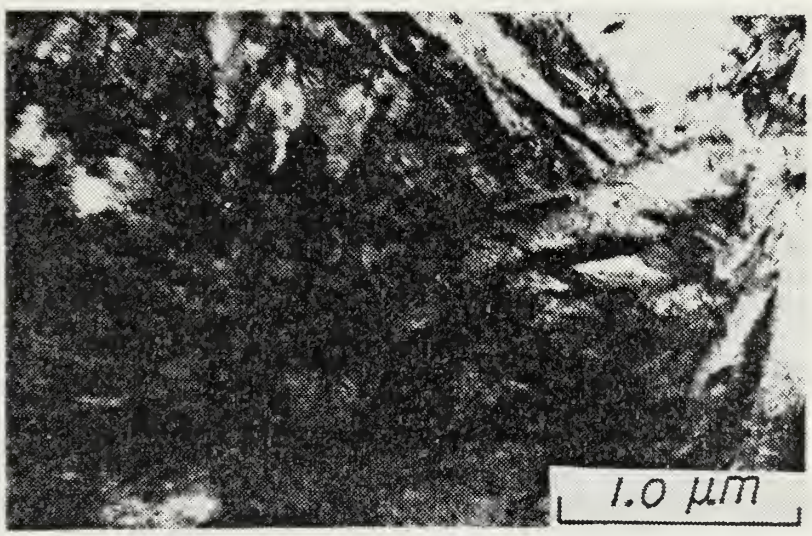

(f)

Figure 24. (CONTINUED)

2. Location B'

Location B' is in the base metal very near the visible heat affected zone of the non-preheated sample. Optical investigation shows a similar appearance in B' as that found in A', Figure 25. The SEM micrographs at 2000X, Figure 26, reveals a microstructure very similar to that of the base metal. The microstructure as observed by transmission electron microscopy is comprised of heavily tempered martensite, and a mixture of fine and coarse temper carbides from the original heat treatment, Figures 27(a-f). The martensite laths average width in Location B' is 0.3 microns. A higher dislocation density with evidence of sub-grain formation was observed that was not seen in the similar Location B in the preheated weldment.

3. Location C'

Location C', the grain refined heat affected zone, is illustrated in Figure 25 forming a visible boundary line with the much coarser microstructure of the base metal, Location B'. The higher magnification scanning electron microscopic investigation reveals a mixture of newly transformed martensite and the original tempered structure with many large carbides, Figure 28. The dominant microstructure in the transmission electron microscopic observations is the original tempered microstructure with fine lath heavily dislocated martensite with some transformation twinning. The mottled surface shown in Figures 29(a-f) is due to

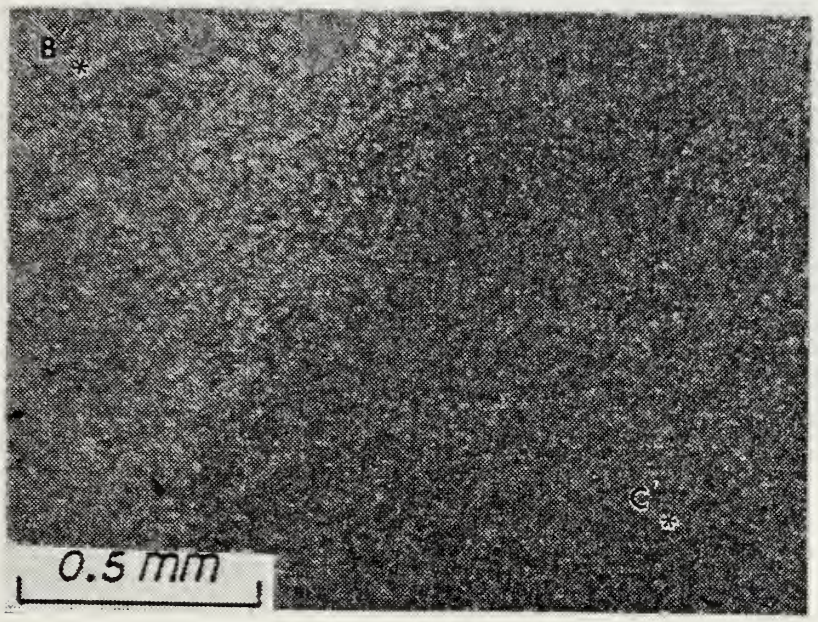

Figure 25. Optical Micrograph of Locations B' and C'

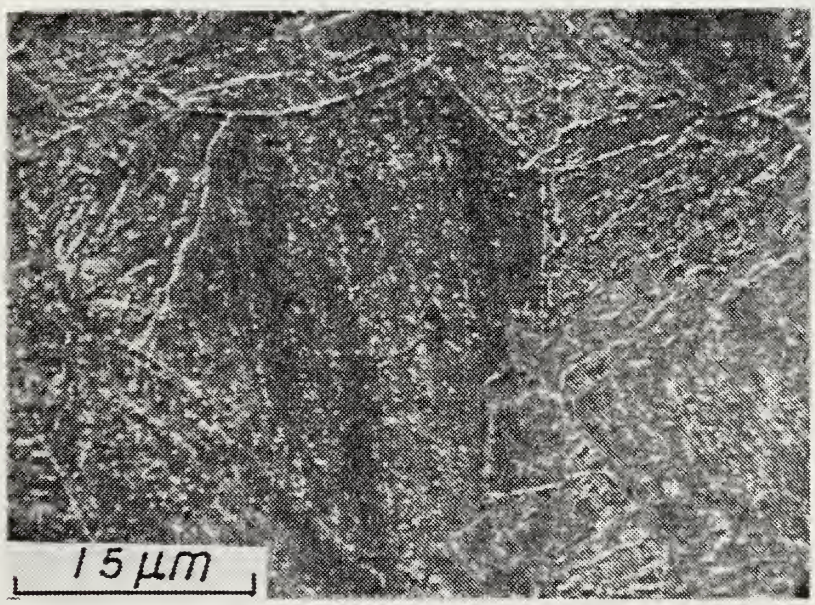

Figure 26. SEM Micrograph of Location B'

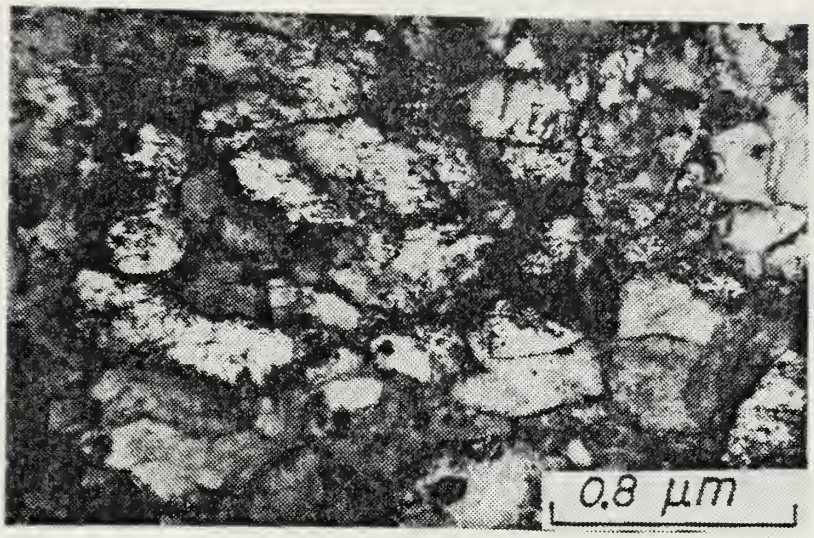

(a)

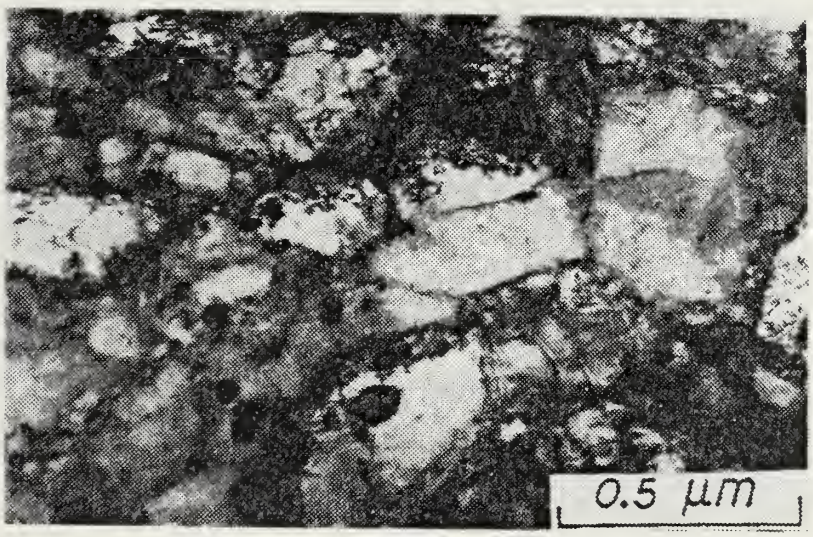

(b)

Figure 27. TEM Micrographs of Location B'

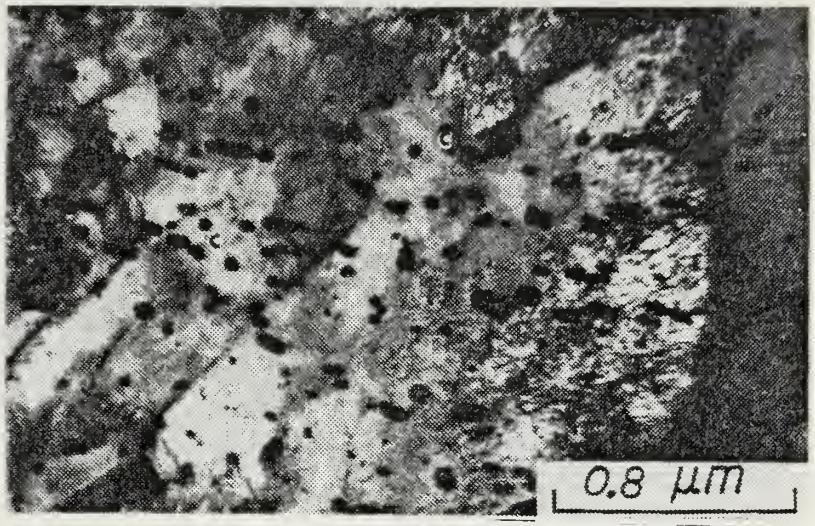

(c)

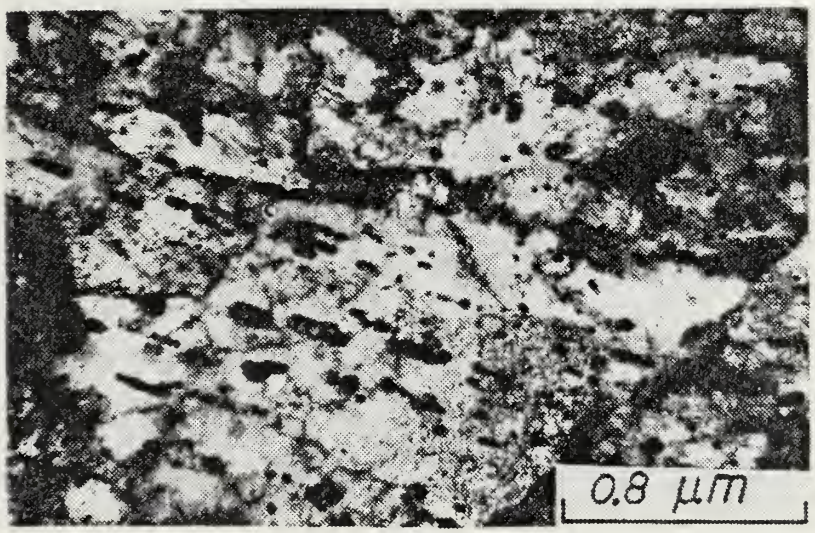

(d)

Figure 27. (CONTINUED)

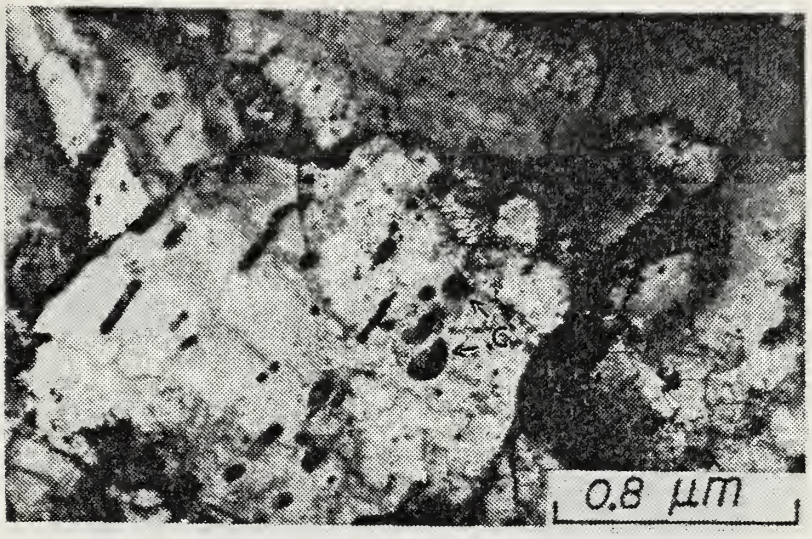

(e)

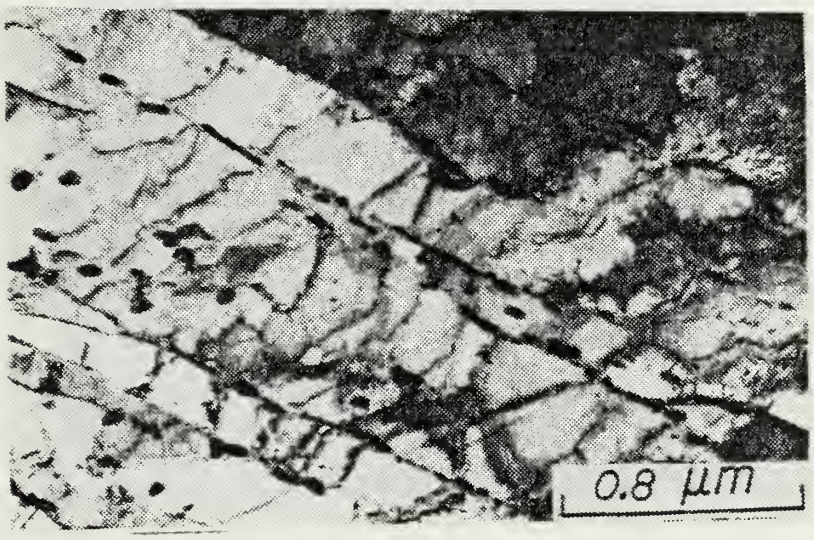

(f)

Figure 27. (CONTINUED)

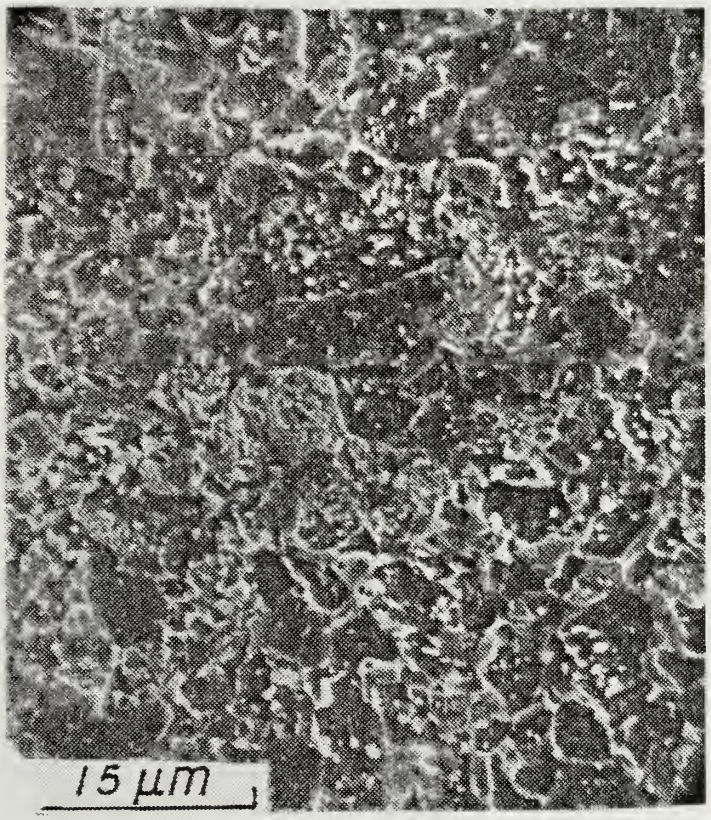

Figure 28. SEM Micrograph of Location C'

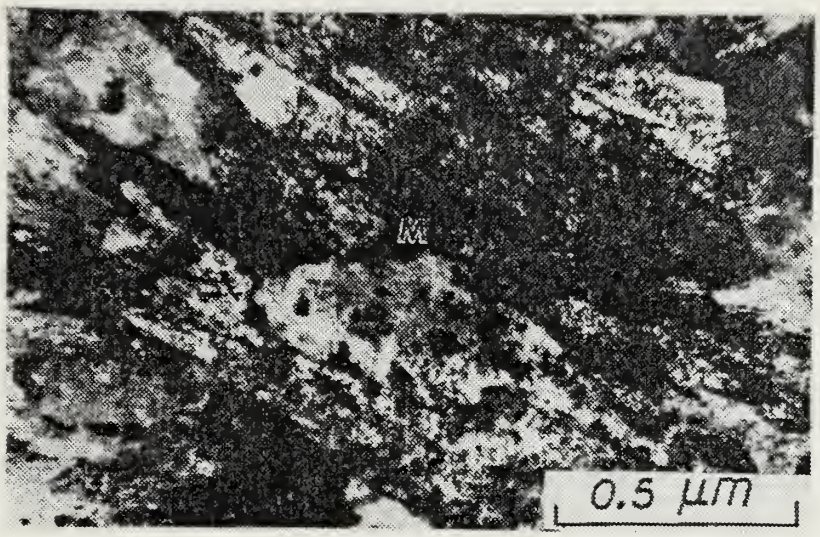

(a)

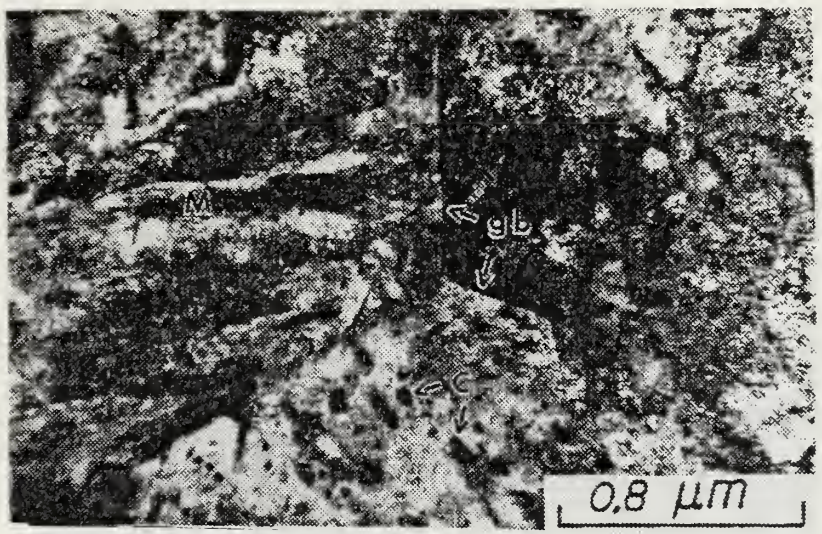

(b)

Martensite (M)

Temper Carbides (C)

Figure 29. TEM Micrographs of Location C'

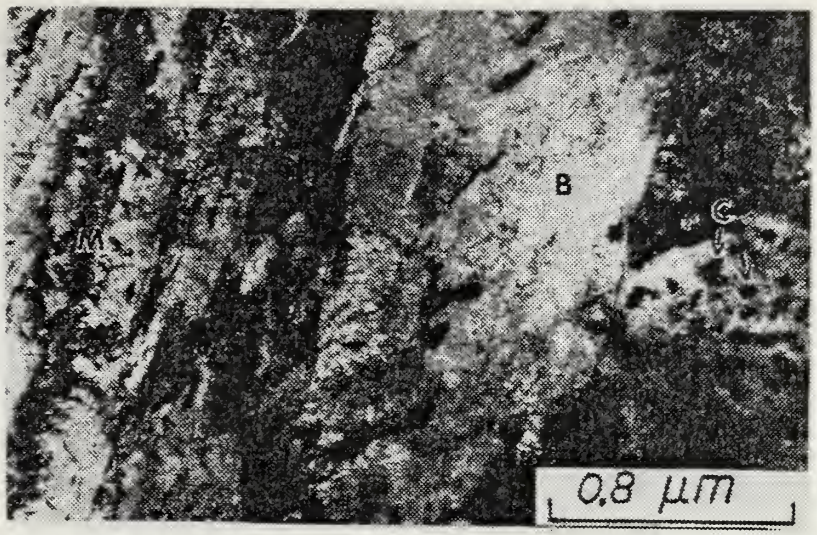

(c)

Martensite (M)

Bainite (B)

Temper Carbides (C)

(d)

Figure 29. (CONTINUED)

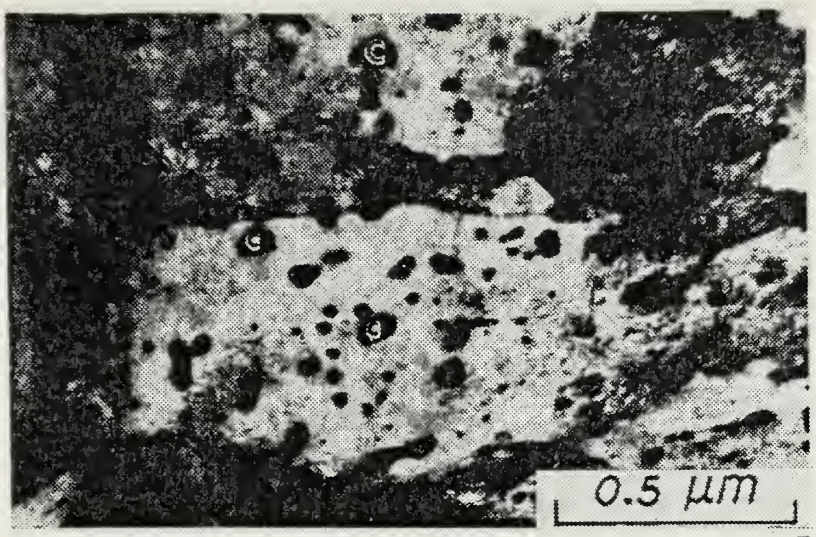

(e)

(f)

Moddled surface is an artifact due to specimen contamination

Figure 29. (CONTINUED)

surface contamination of the thin foil specimen. The previously observed temper carbides are still present while the average martensite lath width is 0.2 microns.

4. Location D'

Location D' like that of Location D was selected from the grain coarsened heat affected zone near the visible fusion line. The microstructure is martensitic in nature as shown in the optical micrograph of Figure 30. The scanning electron micrograph in Figure 31 shows mainly newly transformed martensite with perhaps small regions of the original tempered structure. The detail of the microstructure becomes evident in the TEM observations, Figures 32(a-f). The microstructure is a combination of autotempered martensite, fine lath heavily dislocated martensite (lath width average, 0.1 microns), and still some of the original large temper carbides. The martensite displays a significant amount of transformation twinning.

5. Location E'

The alloying region of the as cast weld metal of the non-preheated sample is designated E'. The microstructure observed by optical, scanning electron, and transmission electron microscopy were the same as E, Figures 22, 23 and 24(a-f).

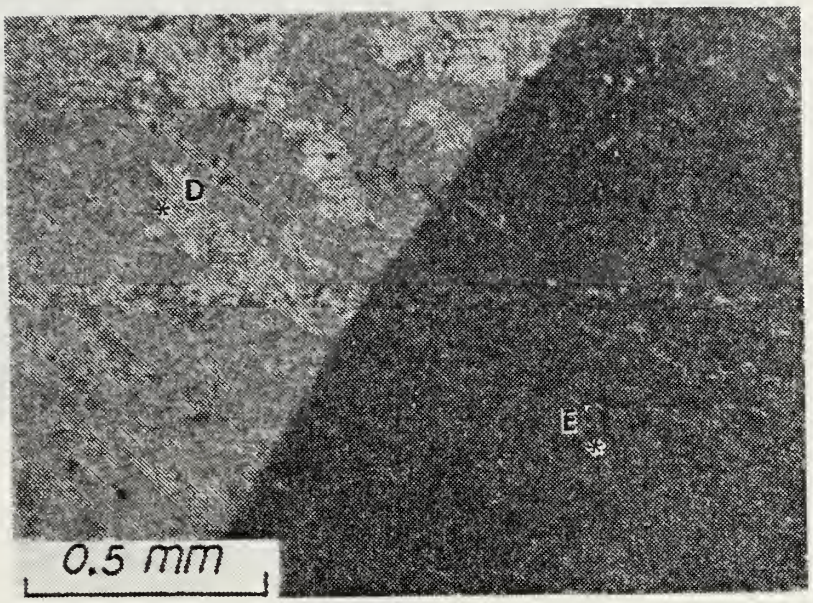

Figure 30. Optical Micrograph of Locations D' and E'

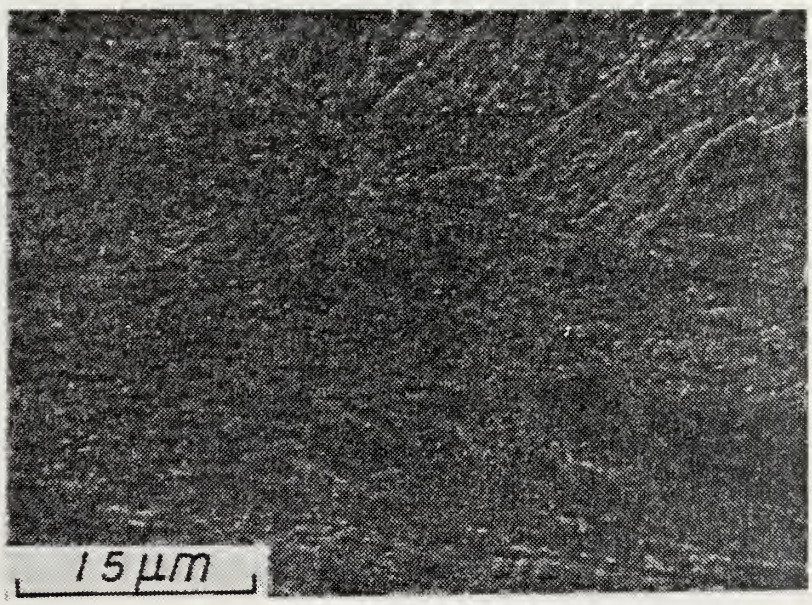

Figure 31. SEM Micrograph of Location D'

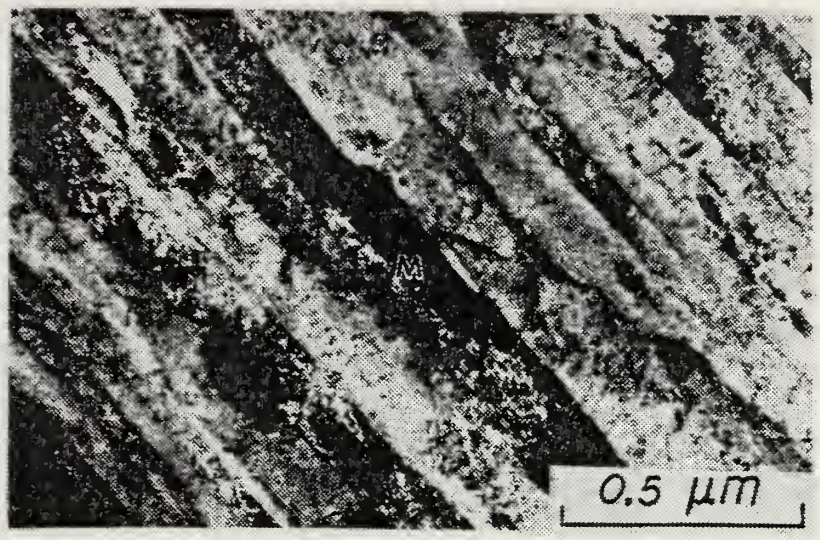

(a)

Newly Transformed Martensite (M)

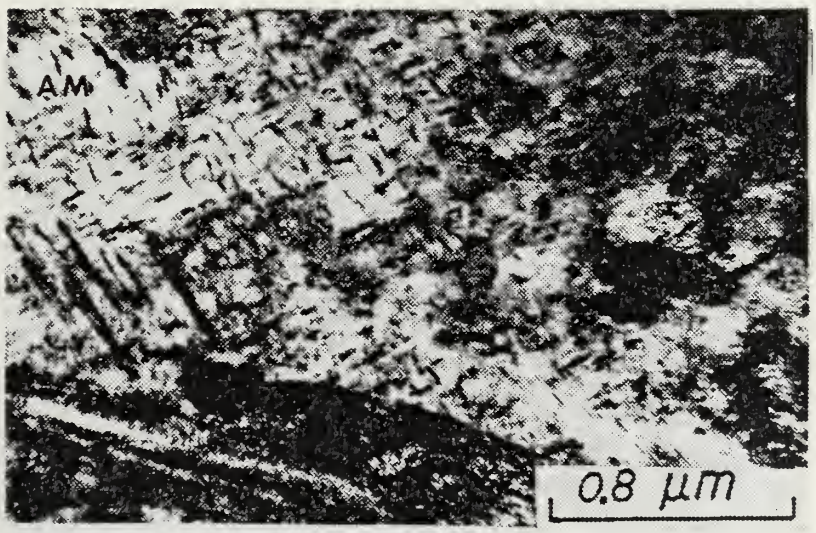

(b)

Transformation Twinning in Auto-tempered Martensite

Figure 32. TEM Micrographs of Location D'

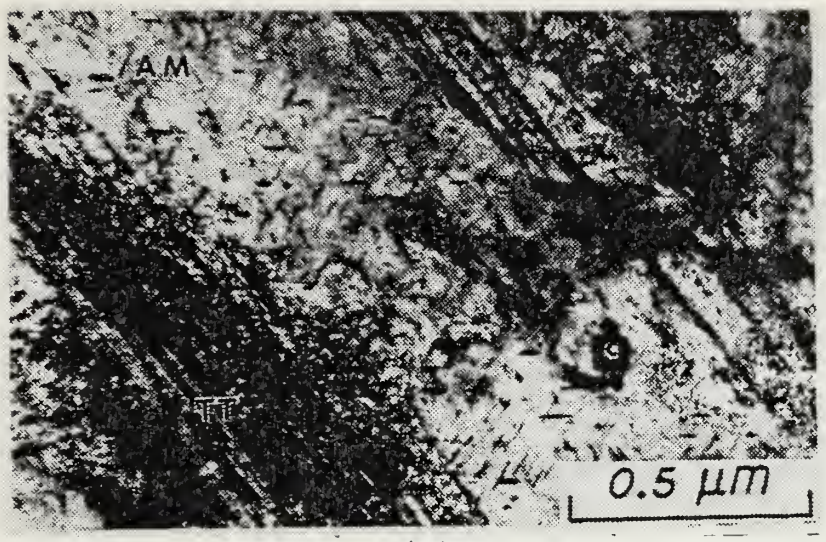

(c)

Transformation Twinning in Auto-tempered Martensite

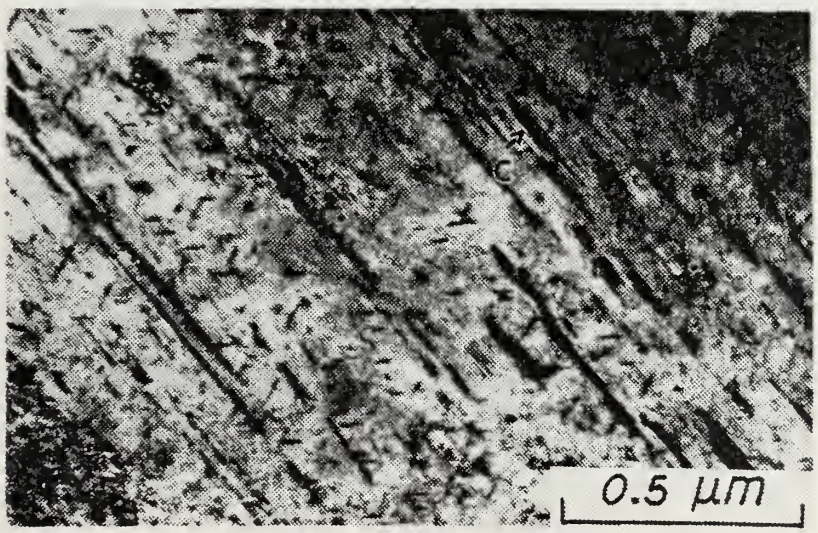

(d)

Temper Carbides (C)

Figure 32. (CONTINUED)

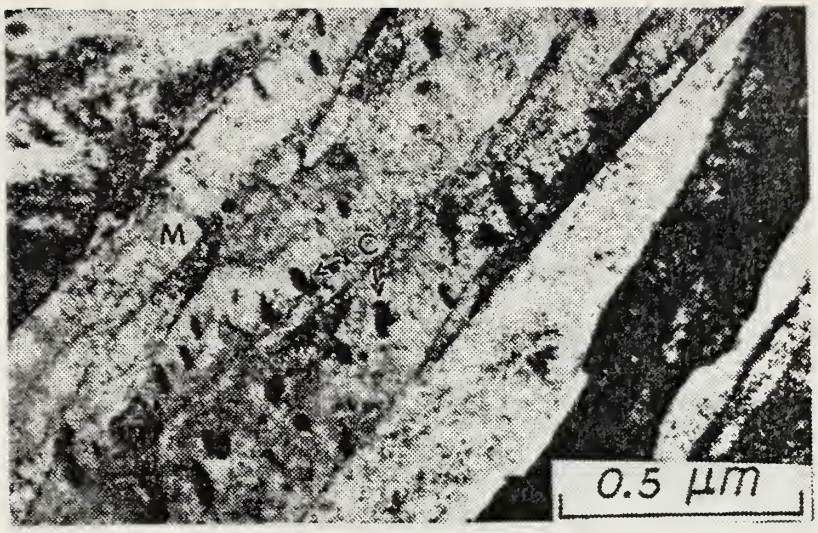

(e)

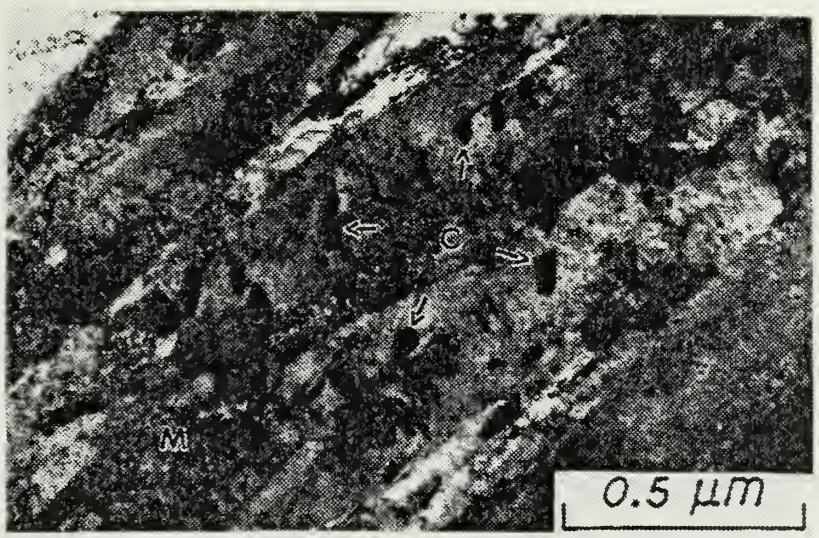

(f)

Temper Carbides (C)

Figure 32. (CONTINUED)

V. DISCUSSION

A. MICROSTRUCTURE

1. Changes in Temper Carbides

The average diameter of the temper carbides were determined for each location and plotted in Figures 33 and 34. Due to the amount of scatter in the measured diameters of the temper carbides, it can be concluded that the size does not change. However, the number density appears to decrease as the fusion line was approached. One major difference between the preheated and non-preheated samples is the fact that some of these large carbides remain undissolved in Location D' (0.5 millimeters from the fusion line in the non-preheated sample). This is presumably due to the very short time spent at the elevated temperature before the weldment is rapidly cooled. The carbides are expected to dissolve at the A_{c1} (650° C) temperature. However, due to the inherent rapid heating and cooling that occurs during welding, they persist to very much higher temperatures.

The presence of these undissolved carbides results in the overall reduction in the carbon content of the austenite and this will alter both the M_s temperature and the hardenability [Ref. 29]. This decreased carbon content of the austenite will raise the M_s temperature and reduce the hardenability.

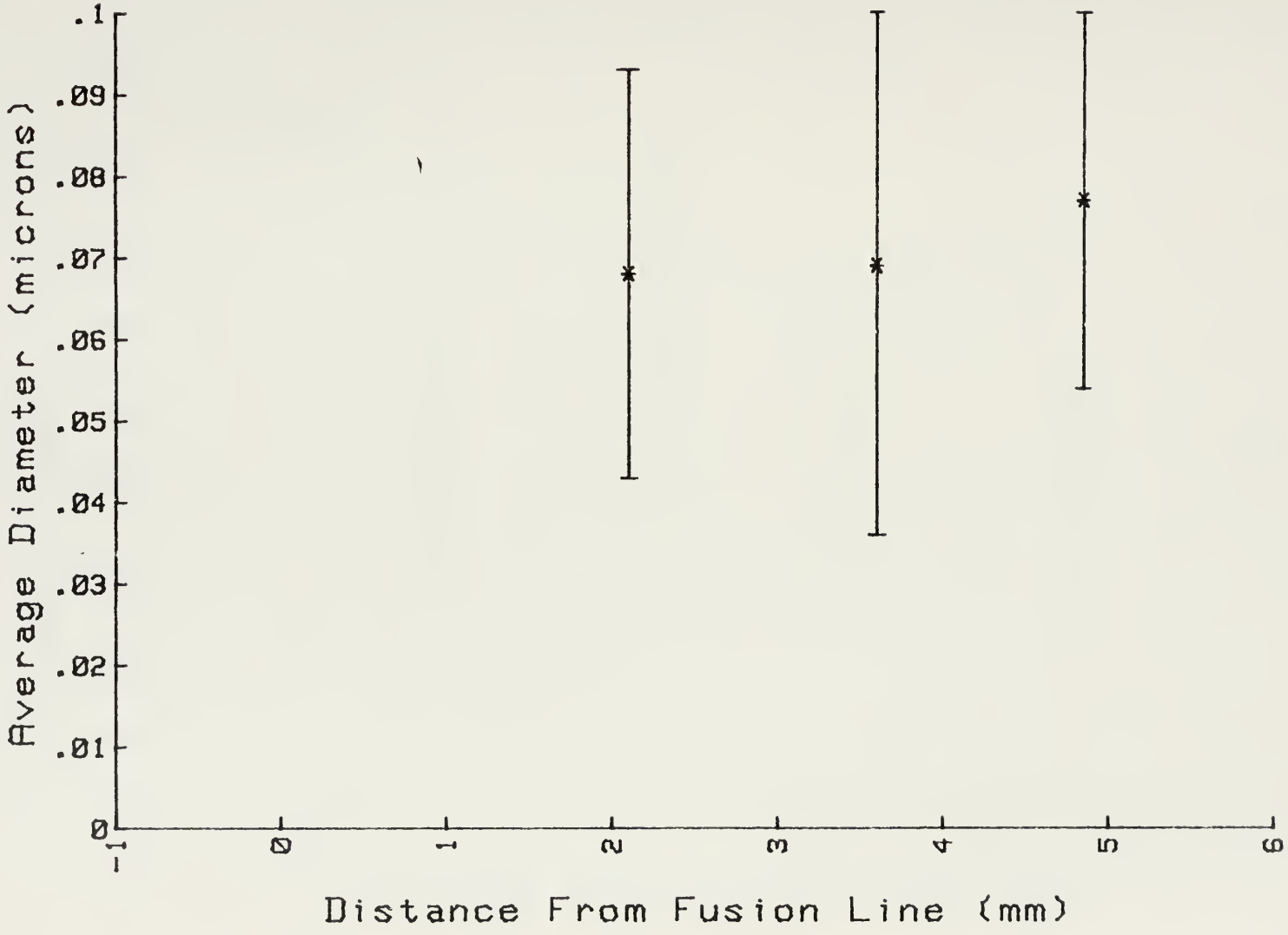

Figure 33. Average Diameter of Preheated Temper Carbides

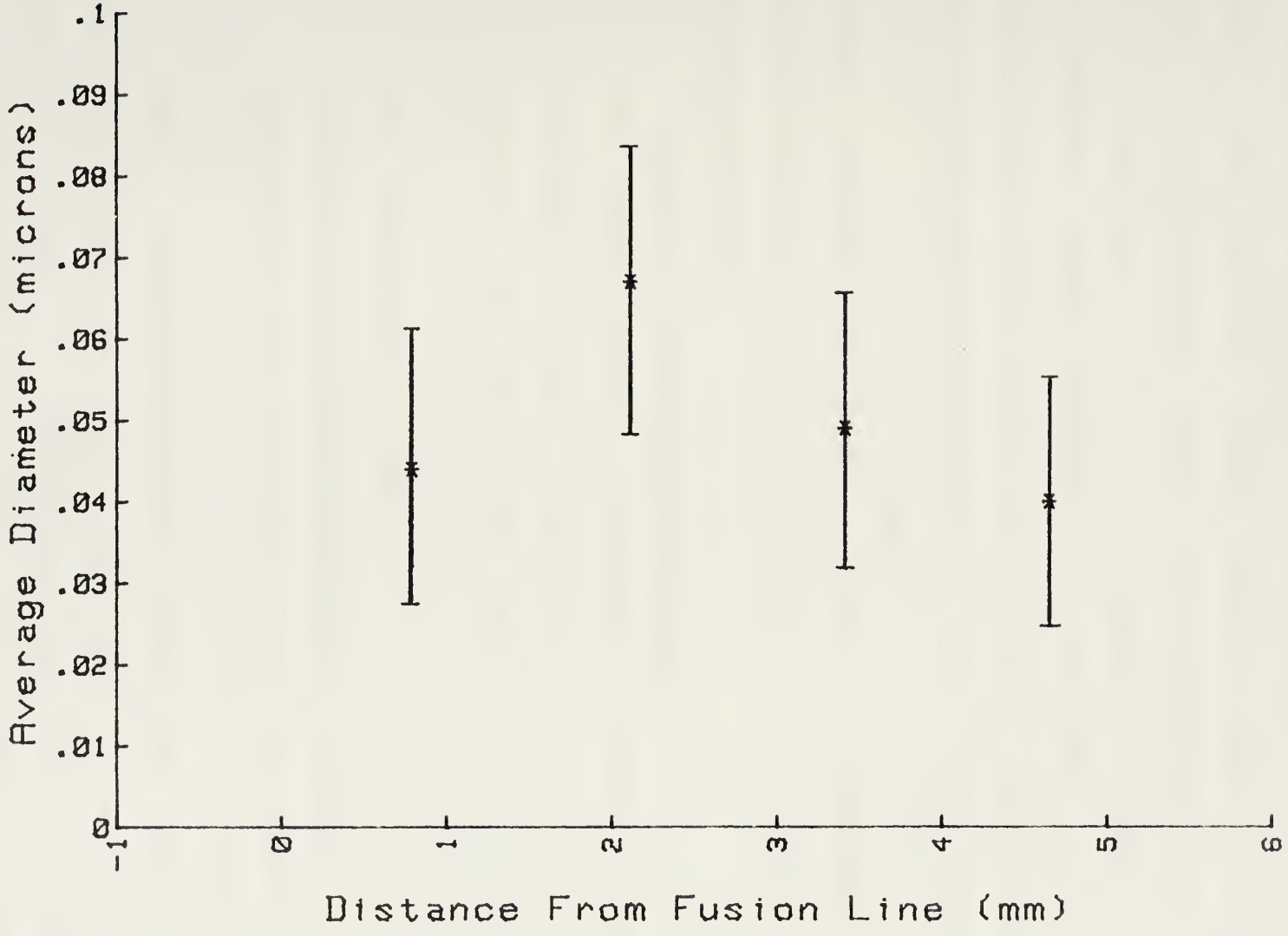

Figure 34. Average Diameter of Non-Preheated Temper Carbides

The significant difference between the preheated and non-preheated weldments was the existence of these temper carbides much closer to the fusion line in the non-preheated sample. Also, the higher number density of these carbides across the heat affected zone of the non-preheated sample than corresponding locations in the preheated specimen. The presence of preheat results in not only higher peak temperatures, but also longer time at elevated temperatures during welding which should result in more carbide dissolution. This can explain the difference in the hardness gradients, Figures 8 and 9, as the martensite formed upon cooling with preheat should have a higher carbon content than without preheat.

2. Presence of Transformation Twinning

The greater amount of transformation twinning present in the non-preheated sample is probably due to more rapid cooling [Ref. 30], and local carbon segregation following carbide dissolution due to less time at the peak temperature and the more rapid quench, Figure 32.

3. Relative Distribution of Martensite in the HAZ

The volume fraction of newly transformed martensite versus the surviving original tempered structure changed as a function of the distance from the fusion line. Qualitatively the volume fraction of the surviving original tempered structure increased with distance from the fusion line due to incomplete transformation of the tempered ferrite/carbide

composition to austenite. This is due to the very short time spent at the peak temperature during welding. The non-preheated weldment retains the original tempered microstructure much closer to the fusion line than the preheated due to an even more rapid cooling following welding resulting in less time available for the transformation of ferrite and carbides to austenite. This also contributes to the lower hardness of the non-preheated heat affected zone.

Heavily dislocated martensite exists in both the preheated and non-preheated heat affected zones near the base metal whereas autotempered martensite was frequently observed near the fusion line. The lack of autotempering near the base metal may explain the higher hardness of this region when compared to the hardness near the fusion line (where autotempering is observed) for the preheated sample.

4. Martensite Lath Width

The heavily dislocated martensite has a much smaller lath width than the autotempered martensite indicating that it formed at a lower temperature. Additionally the coarse laths only appear in the coarse grained region of the heat affected zone. Thus the coarse austenite grains that form near the fusion line result upon cooling is first the transformation of the coarse laths which subsequently autotemper followed by the formation of the fine lath heavily dislocated martensite at lower temperatures where there is insufficient time at temperature for the autotempering to

occur. Plots of the martensite lath size as a function of distance from the fusion line are shown in Figures 35 and 36.

5. Hydrogen Induced Cold Cracking

The only reason for concern from a microstructural point of view is the increased incidence of transformation twinned martensite in the non-preheated weldment. Transformation twinned martensite is the most susceptible microstructure to hydrogen induced cold cracking when in the presence of hydrogen and stresses near the yield stress of the material. There is, however, some twinning present in both weld specimens but it is still only a small volume fraction even in the non-preheated weld, so the major difference in hydrogen assisted cracking, if there is a difference, will probably be due to the amount of hydrogen present during the welding.

There is no reason to expect that the microstructures resulting from the preheated weld will be much different in the susceptibility to hydrogen assisted cracking than the non-preheated. In fact the more gradual change in hardness in the heat affected zone to base metal region may be beneficial.

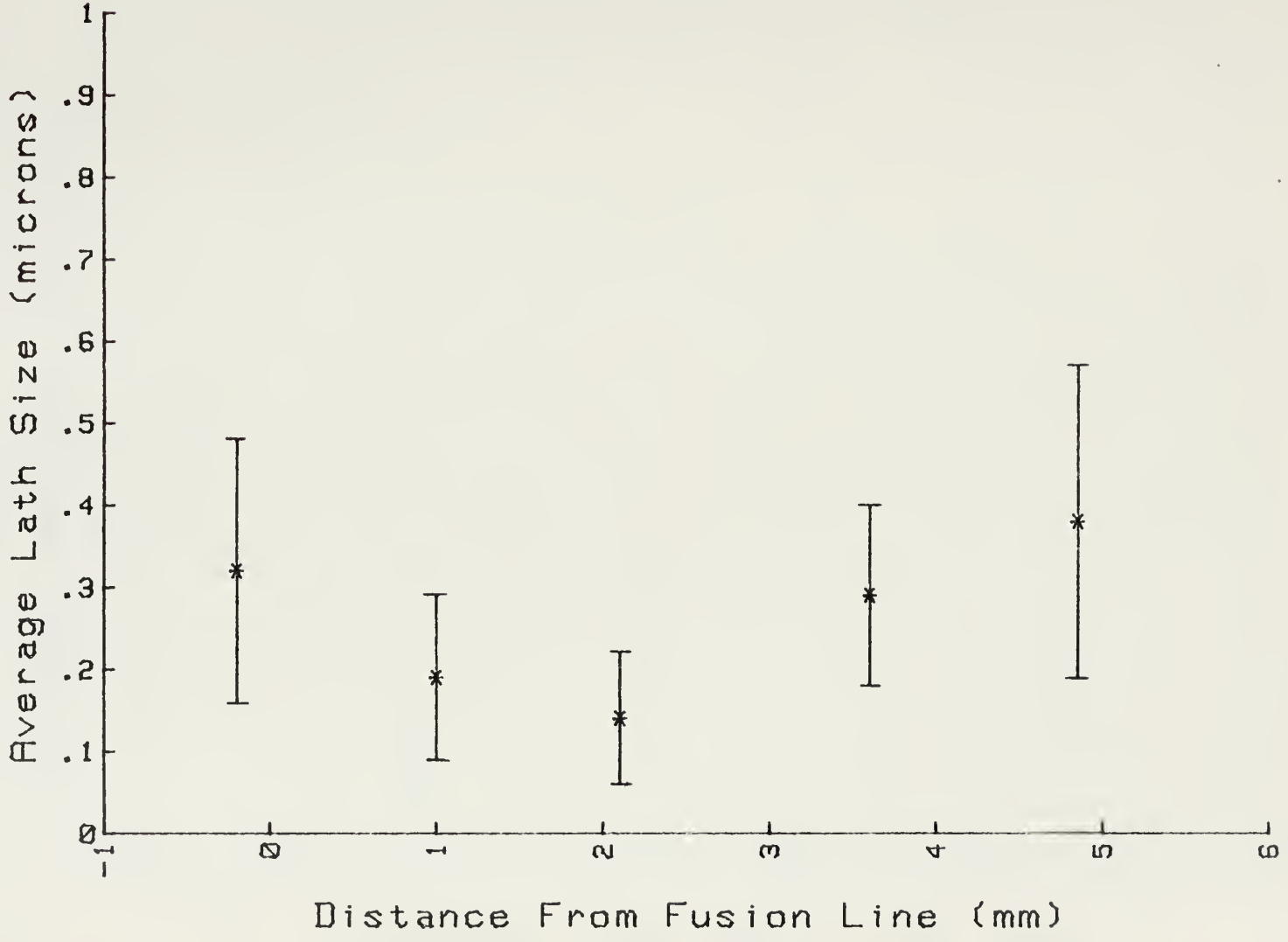

Figure 35. Average Martensite Lath Width of the Preheated Weldment

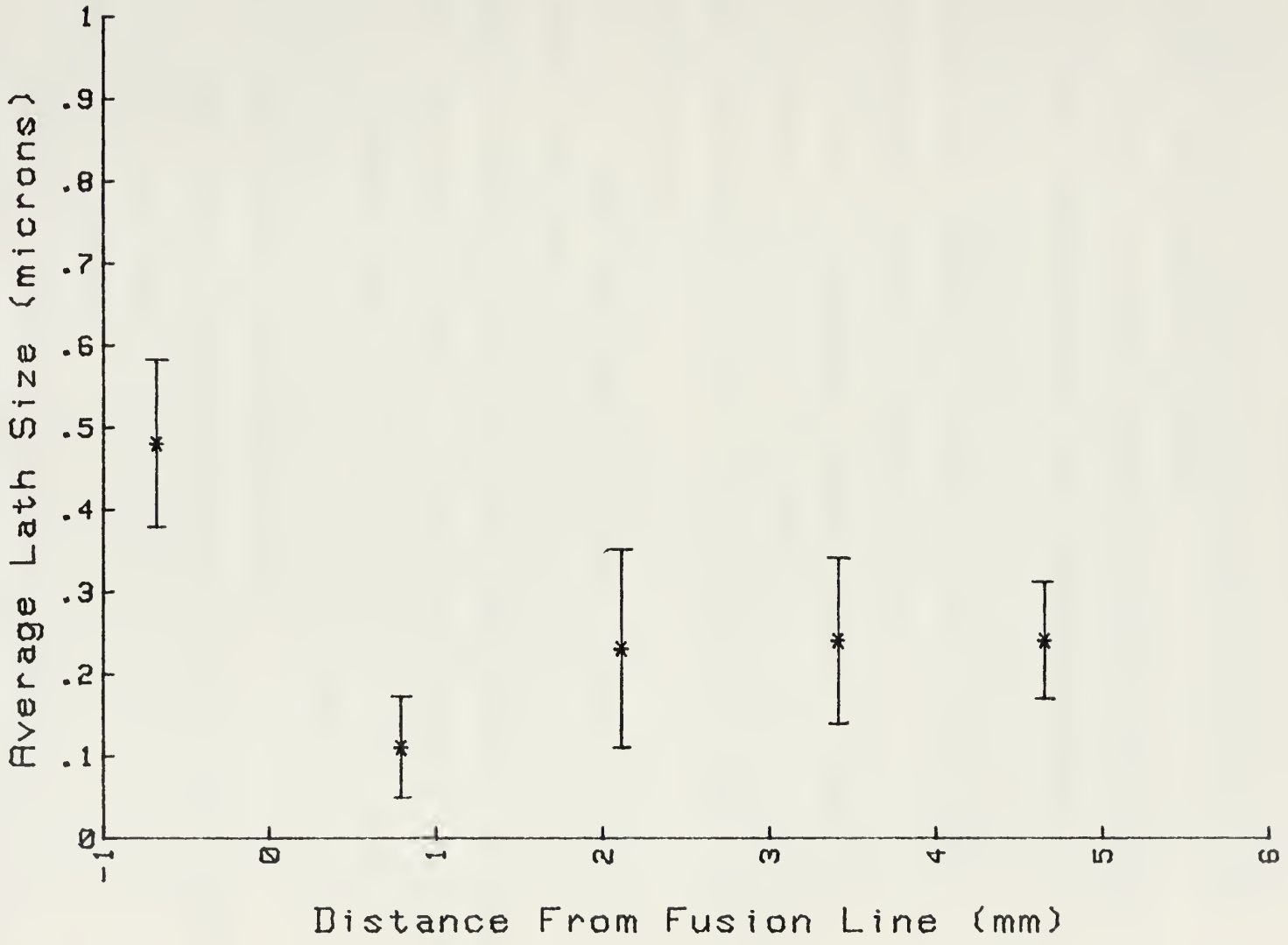

Figure 36. Average Martensite Lath Width of the Non-Preheated Weldment

VI. CONCLUSIONS

Based on the research and the results obtained, the following conclusions are drawn:

1. There is a severe hardness gradient near the edge of the heat affected zone of the preheated weldment. The high hardness remains nearly constant across the heat affected zone, dropping to similar levels of the base metal hardness in the as cast weld metal.

2. There is a gradual hardness gradient across the heat affected zone of the non-preheated sample which reaches a peak value nearly the same as the preheated sample near the fusion line.

3. The rapid heating/cooling that occurs in the heat affected zone results in the retention of the original tempered microstructure after peak temperatures considerably higher than the A_1 (650° C). This lack of carbide dissolution in the preheated sample persists to about 1.5 millimeters from the fusion line whereas it persists right up to the fusion line for the non-preheated weld.

4. The lack of carbide dissolution in the heat affected zone of the non-preheated weld results in the lower heat affected zone hardness.

5. The only difference in the microstructures other than the amount of carbide dissolution is that the non-preheated

sample contains slightly more internally twinned martensite than the preheated sample. This is probably due to a combination of the more rapid cooling rate and a greater inhomogeneity of the carbon once the carbides dissolve.

VII. RECOMMENDATIONS

Based on the research conducted, the results obtained and the conclusions drawn, the following recommendations are offered:

1. A microstructural analysis and comparison between a preheated and non-preheated single weld bead be conducted to isolate the preheating effects from the thermal effects of previous weld beads.

2. Preheated and non-preheated HY-80 steel weldments be prepared in a hydrogen free environment and tested mechanically to determine strength, fracture toughness and crack initiation and propagation property comparisons.

LIST OF REFERENCES

1. Department of the Navy Military Specification MIL-E-19322 Military Specification Fabrication, Welding, and Inspection of HY80/100 Submarine Hulls.

2. Department of the Navy Military Specification MIL-S-16216A (SHIPS), "Military Specification Steel Plate, Alloy, Structural, High Yield Strength [HY-80 and HY-100]," (15 March 1972).

3. Connor, L.P., Rathbone, A.M., Willebrand, C.F., "Effects of Composition on Heat Affected Zone Toughness of Ni-Cr-Mo Steel Weldments," U.S. Steel Applied Research Lab Report 39, 018-008, pp. 16-17 (Oct. 21, 1965).

4. Emmanuel, G.N., Young, D.E., Spaks, G.L., "The Metallurgy of Well Heat-Affected Zones in HY-80 High Strength Steel," Metals Engineering Quarterly 1(3), 82-87 (1961).

5. U.S. Coast Guard Solicitation RFP-CG-80588-A, project SR-1256 (Nov. 14, 1977).

6. Metals Engineering Quarterly, 1(3), 82-87 (1961).

7. Welding Journal, 41(8), 375s-384s (1962).

8. Ibid, 43(6), 265s-28ls (1964).

9. Ibid, 45(9), 393s-400s (1966).

10. Spahr, G.L., "An Investigation of the Weldability of HY-80 Steel," The Babcokc and Wilcox Company, Barbarton, Ohio, Navy Contract NO6s-84169 (March 16, 1961).

11. Schreitz, W.G., "Restraint Cracking Technique for use in Simulated Weld Thermal Cycling Studies," U.S. Navy Marine Laboratory, Annapolis, Maryland, MEL R&D Report 90/64 (June 26, 1964).

12. Thompson, R.G., "The Study of Hot Cracking in Welded High-Strength Steel Using the Varestraint Test," U.S. Navy Marine Laboratory, Annapolis, Maryland, Phase Report 13/67 (March, 1967).

13. Smith, E., "Effect of Welding and Post-Weld Heat-Treatment on HY-80 and Q1(N) Steels," Welding and Metal Fabrication, Vol. 40, No. 5, p. 177-183 (May 1972).

14. Flax, F.W., Keith, R.G., and Randall, M.D., "Welding the HY Steels," ASTM Special Technical Publication 494, American Society for Testing and Materials, Philadelphia, PA (1971).

15. Savage, W.F., Nippes, E.F., and Szekeres, E.S., "A Study of Weld Interface Phenomena in a Low Alloy Steel," Welding Research Supplement, 260s (September 1976).

16. Dolby, R.E., "Cracking in Weldments of Structural Steels," Engineering Application of Fracture Analysis, 1st National Conference on Fracture, Tokannisburg, SA, p. 313-322 (November 1979).

17. Boniszewski, T. and Watkinson, F., "Effect of Weld Microstructures on Hydrogen-Induced Cracking in Transformable Steels: Part I and II," Metals and Materials, pp. 90-151 (March 1973).

18. Welding Journal 40(4), 155s-159s (1961).

19. Ibid, 40(4), 175s-181s (1961).

20. Savage, W.F., Nippes, E.F., and Szekeres, E.S., "A Study of Weld Interface Phenomena in a Low Alloy Steel," Welding Research Supplement, 260s (September 1976).

21. Porter, D.A., and Easterling, K.E., "Phase Transformations in Metals and Alloys," Van Nostrand Reinhold Company, New York, p. 376 (1981).

22. Beachem, C.D., "A New Model for Hydrogen-Assisted Cracking (Hydrogen 'Embrittlement')," Metallurgical Transactions, Volume 3, pp. 437-451 (February, 1972).

23. Boniszewski, T. and Watkinson, F., "Effect of Weld Microstructure on Hydrogen-Induced Cracking in Transformable Steels: Part I," Metals and Materials, pp. 90-96 (March 1973).

24. Porter, D.A., and Easterling, K.E., "Phase Transformations in Metals and Alloys," Von Nostrand Reinhold Company, New York, p. 376 (1981).

25. Kaae,J.L., "Mechanical Properties, Microstructure and Susceptibility to Cracking in the HAZ of Controlled-Rolled, Niobium Treated, Low Carbon, Manganese Steels," British Welding Journal, pp. 395-407 (August 1968).

26. Donachie, S.J., and Ansell, G.S., "The Effect of Quench Rate on the Properties and Morphology of Ferrous Martensite," Metallurgical Transactions, Volume 6A, pp. 1863-1875 (October 1975).

27. Speich, G.R., "Tempering of Low Carbon Martensite," AIME, Volume 245, pp. 2553-2563 (December, 1969).

28. Donachie, S.J., and Ansell, G.S., "The Effect of Quench Rate on the Properties and Morphology of Ferrous Martensite," Metallurgical Transactions, Volume 6A, pp. 1863-1875 (October 1975).

29. Porter, D.A., and Easterling, K.E., "Phase Transformations in Metals and Alloys," Van Nostrand Reinhold Company, New York, pp. 383-386 (1981).

30. Boniszewski, T., and Watkinson, F., "Effect of Weld Microstructures on Hydrogen-Induced Cracking in Transformable Steels: Part I," Metals and Materials, pp. 90-96 (February 1973).

INITIAL DISTRIBUTION LIST

		No. Copies
1.	Defense Technical Information Center Cameron Station Alexandria, Virginia 22314	2
2.	Library, Code 0142 Naval Postgraduate School Monterey, California 93943	2
3.	Department Chairman, Code 69 Department of Mechanical Engineering Naval Postgraduate School Monterey, California 93943	1
4.	Associate Professor K.D. Challenger, Code 69Ch Department of Mechanical Engineering Naval Postgraduate School Monterey, California 93943	5
5.	Mr. Gene L. Franke, Code 2821 David Taylor Research and Development Center Annapolis, Maryland 21402	1
6.	Mr. Richard J. Wong, Code 2821 David Taylor Research and Development Center Annapolis, Maryland 21402	1
7.	LCDR David R. Clark, USN c/o Murphy 15 Delaware Ave. Bath, New York 14810	2
8.	Mr. C. Zanis, Code 2821 David Taylor Research and Development Center Annapolis, Maryland 21402	1

200053

Thesis
C4808 Clark
c.1 Characterization of preheated and non-preheated HY-80 steel weldments by transmission electron microscopy.

22 MAR 87 31137

200053

Thesis
C4808 Clark
c.1 Characterization of preheated and non-preheated HY-80 steel weldments by transmission electron microscopy.

AMERICAN BINDERY TOPEKA KANSAS

thesC4808
Characterization of preheated and non-pr
3 2768 002 10257 6
DUDLEY KNOX LIBRARY